

## Development of L-Amino Acid Based Hydroxyl Functionalized Biodegradable Amphiphilic Polyesters and Their Drug Delivery Capabilities to Cancer Cells

Sonashree Saxena, and Manickam Jayakannan

*Biomacromolecules*, **Just Accepted Manuscript** • DOI: 10.1021/acs.biomac.9b01124 • Publication Date (Web): 08 Oct 2019

Downloaded from [pubs.acs.org](https://pubs.acs.org) on October 13, 2019

### Just Accepted

“Just Accepted” manuscripts have been peer-reviewed and accepted for publication. They are posted online prior to technical editing, formatting for publication and author proofing. The American Chemical Society provides “Just Accepted” as a service to the research community to expedite the dissemination of scientific material as soon as possible after acceptance. “Just Accepted” manuscripts appear in full in PDF format accompanied by an HTML abstract. “Just Accepted” manuscripts have been fully peer reviewed, but should not be considered the official version of record. They are citable by the Digital Object Identifier (DOI®). “Just Accepted” is an optional service offered to authors. Therefore, the “Just Accepted” Web site may not include all articles that will be published in the journal. After a manuscript is technically edited and formatted, it will be removed from the “Just Accepted” Web site and published as an ASAP article. Note that technical editing may introduce minor changes to the manuscript text and/or graphics which could affect content, and all legal disclaimers and ethical guidelines that apply to the journal pertain. ACS cannot be held responsible for errors or consequences arising from the use of information contained in these “Just Accepted” manuscripts.

# Development of L-Amino Acid Based Hydroxyl Functionalized Biodegradable Amphiphilic Polyesters and Their Drug Delivery Capabilities to Cancer Cells

Sonashree Saxena and Manickam Jayakannan\*

Department of Chemistry

Indian Institute of Science Education and Research (IISER), Pune

Dr. Homi Bhabha Road

Pune 411008, Maharashtra, India

Corresponding Author: E-mail: [jayakannan@iiserpune.ac.in](mailto:jayakannan@iiserpune.ac.in)

Keywords

Functional Polyesters, L-Amino acids, Enzyme-responsive, Biodegradable polyesters, Nano-assemblies, Drug Delivery.

## Abstract

Hydroxyl-functionalized amphiphilic polyesters based on L-amino acid bio-resources were designed and developed and their nano-assemblies were explored as intracellular enzyme-biodegradable scaffolds for delivering anticancer drugs and fluorophores to cancer cells. To accomplish this task, acetal-masked multi-functional dicarboxylic ester monomer from L-aspartic acid was tailor-made and it was subjected to solvent-free melt transesterification polycondensation with commercial diols to produce acetal-functionalized polyesters. Acid-catalyzed post-polymerization de-protection of these acetal-polyesters produced amphiphilic hydroxyl-functionalized polyesters. The amphiphilic polyesters were self-assembled in

aqueous medium to produce nanoparticles of size < 200 nm. Wide ranges of both water-soluble and water-insoluble anticancer drugs such as doxorubicin (DOX), camptothecin (CPT) and curcumin (CUR) and fluorophores such as Nile red (NR), Rose Bengal (RB) and Congo red (CR) were encapsulated in hydroxyl polyesters nanoparticles. *In vitro* drug release studies revealed that the aliphatic polyester backbone underwent lysosomal enzymatic-biodegradation to release the loaded cargoes at the intracellular compartments. LysoTracker assisted live-cell confocal microscopy studies further confirmed the co-localization of the polymer nano-scaffolds in the lysosomes and supported their enzymatic-biodegradation for drug delivery. *In vitro* cytotoxicity studies showed that the nascent polymers were not toxic whereas their anticancer drug-loaded nanoparticles exhibited excellent cell killing in cervical cancer (HeLa) cell lines. The drug (CPT, CUR, and DOX) and the fluorophores (NR, RB, and CR) loaded polymer nanoparticles were highly luminescent; thus, the encapsulated polymer nanoparticles enabled the multiple color-tunable bio-imaging in cancer cells in the entire visible region from blue to deep red. Time-dependent live-cell confocal microscopy studies established that the cellular uptake of drugs and fluorophores were accomplished 5 to 10 folds higher while they were delivered from the hydroxyl polyester platform. The hydroxyl polyester nano-carrier design strategy opens up new opportunities in drug delivery to cancer cells from biodegradable polymer platform based on L-amino acids.

## Introduction

Synthetic polymers based on bio-resources are emerging as very important biomaterials due to their excellent biocompatibility under physiological conditions and the availability of the abundant raw materials, and so on so forth.<sup>1-4</sup> L-Amino acid bio-resources have unique features in terms of functional group diversity such as carboxylic acid, amine, hydroxyl, aryl substitution, phenolic, heterocyclic, etc; thus, they provide unlimited opportunities to make bio-degradable and biocompatible polymeric materials.<sup>5-8</sup> Ring-opening polymerization (ROP) is one of the widely employed synthetic routes for L-amino acid resources to make high molecular weight neutral and charged polypeptides,<sup>9-11</sup> di- and tri-block copolymers,<sup>12-13</sup> poly( $\alpha$ -hydroxy acid)s,<sup>14-15</sup> etc. These synthetic polypeptides exhibited both  $\alpha$ -helix and  $\beta$ -sheet secondary structures as similar to that of proteins. The polypeptides were explored for biomedical applications in drug and gene delivery, tissue engineering, and reinforced nanocomposites in bone replacement, etc.<sup>16-18</sup> In the last two decades polycondensation

1  
2  
3 approaches have been developed to construct non-peptide polymer analogs from L-amino  
4 acid resources for biomedical application.<sup>7</sup> Some of the most important non-peptide polymers  
5 are poly(ester-amide)s,<sup>19-23</sup> polycarbonates,<sup>24-29</sup> poly(ester-urethane-urea),<sup>30-33</sup> poly(ester-  
6 urea),<sup>34-39</sup> poly(disulfide-urethane)s,<sup>40-42</sup> poly(acetal-urethane)<sup>43</sup> etc. We have reported melt  
7 polycondensation route to make linear poly(ester-urethane)s<sup>44-46</sup> hyperbranched poly(ester-  
8 urethane)s,<sup>47</sup> amine and disulfide functionalized polyesters,<sup>48-49</sup> pH and enzyme-responsive  
9 aliphatic polyesters<sup>50</sup> and thermo-responsive poly(ester-urethane)s<sup>51</sup> and polyurethanes,<sup>52</sup> etc.  
10 Lysosomal enzymes like esterase, trypsin, and  $\alpha$ -chymotrypsin, etc were found to be efficient  
11 in the biodegradation of the non-peptide polymer nano-assemblies under physiological  
12 conditions.<sup>53,54</sup> Enzyme-responsiveness was explored as a trigger in delivery of anticancer  
13 drugs,<sup>23,29,40,50-52</sup> FRET-based bio-imaging,<sup>54-55</sup> and tissue-fillers,<sup>56-58</sup> etc. Unambiguously, the  
14 amphiphilicity in both peptide and non-peptide polymer systems were largely accomplished  
15 by the introduction of polyethylene glycols (PEG) in the polymer matrix. Though PEG-unit is  
16 an excellent choice in nano- design; they are non-functional which restrict their feasibility for  
17 anchoring targeted ligands and drugs, etc until otherwise tedious and multi-step synthetic  
18 efforts are taken. This emphasized that the design and development of functional  
19 biodegradable polymers from L-amino acid resources with appropriate solubility (or  
20 dispersibility) in aqueous medium could open new generation of polymer structures for their  
21 long-term utility in the biomedical field. Unfortunately, functional non-peptide polymers  
22 from L-amino acid is one of the least explored areas in the literature; thus, new synthetic  
23 efforts are urgently required to address this important problem. This task is addressed in the  
24 present investigation, for the first time, by the design and development of novel hydroxyl  
25 functionalized polyesters from L-amino acid resources. This concept was developed by  
26 cleverly combining the solvent-free melt polycondensation route earlier developed from our  
27 laboratory<sup>44-52</sup> along with the acetal-masking strategy<sup>59-66</sup> in L-aspartic acid system. Acetal-  
28 masking approach has been explored for hydroxyl-functionalized polycaprolactone,<sup>59</sup>  
29 polylactides,<sup>60-61</sup> polyamide,<sup>62</sup> polyurethanes<sup>63-64</sup>, and sugar-based polyester<sup>65-66</sup>; however, up  
30 to our knowledge, it is not explored for L-amino acid polymers to make functional polymers.  
31 To accomplish the above task, new multi-functional monomer based on L-aspartic acid was  
32 designed and it was subjected to melt polycondensation with diols to make new classes of  
33 acetal-functionalized L-aspartic polyesters. Post polymerization de-protection of acetal-  
34 polyester yielded new hydroxyl functionalized amphiphilic polyesters. The hydroxyl  
35 polyester geometry was found to exhibit excellent capability for the encapsulation of wide  
36  
37  
38  
39  
40  
41  
42  
43  
44  
45  
46  
47  
48  
49  
50  
51  
52  
53  
54  
55  
56  
57  
58  
59  
60

ranges of water-soluble and water-insoluble anticancer drugs and fluorophore dyes. The polyester nano-assemblies are enzyme-biodegradable and this new drug delivery concept is schematically shown in Figure 1.

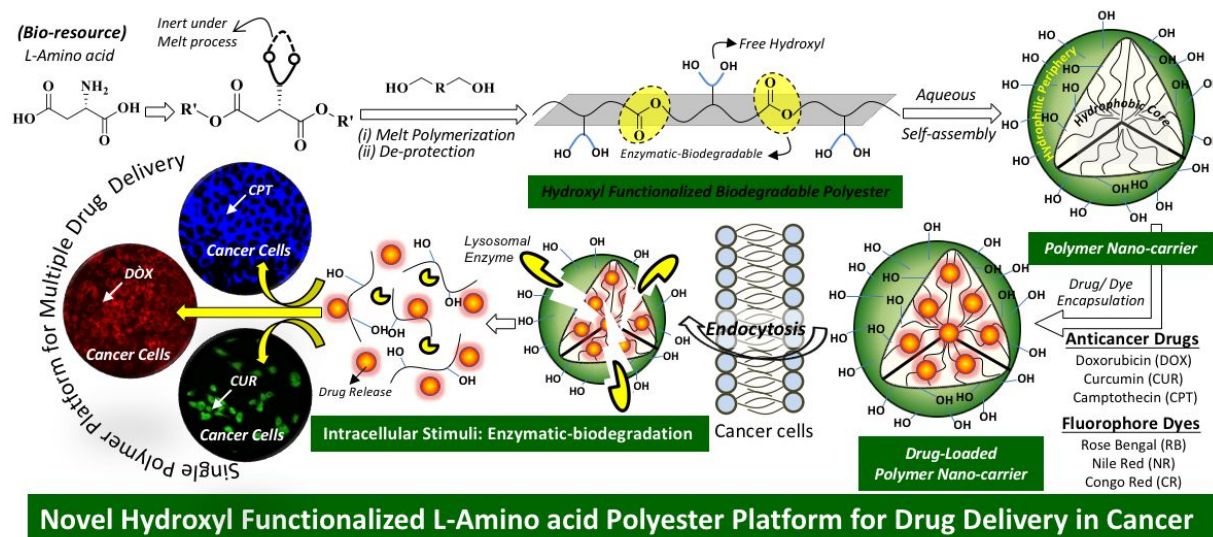


**Figure 1.** Design and development of novel hydroxyl functionalized polyester based on L-amino acid bio-resources and demonstration of their enzyme-responsive drug-delivering capabilities to cancer cells.

Here, hydroxyl functionalized biodegradable amphiphilic polyesters were made through solvent-free melt polycondensation approach and demonstrated their self-assembled nano-scaffold as an enzyme-responsive carrier for delivering multiple drugs to the intracellular compartments of cancer cells. To accomplish this task, the following design parameters were incorporated: (i) multi-functional L-aspartic acid monomer was designed by masking the amine into cyclic-acetal moiety and converting the di-carboxylic acids into di-esters, (ii) under the melt polycondensation process, the acetal unit was found to be inert and it did not interfere during the transesterification of di-ester with commercial diols, (iii) the resultant acetal-containing polyester was de-protected to yield hydroxyl functionalized polyester in which each repeating unit bore bis-hydroxyl functionality to bring hydrophobic-hydrophilic balance for amphiphilicity in the resultant polymer structure, (iv) the amphiphilic polymer self-assembled into 250 nm nanoparticle in aqueous medium and exhibited encapsulation of both water-soluble and water-insoluble anticancer drugs or dyes in a single nano-carrier platform which is very rarely found in L-amino acid platform. The structures of the polymers and occurrence of the melt polycondensation process were established. Dynamic light scattering and atomic force microscope were employed to study the self-

1  
2  
3 assembly process. Anticancer drugs doxorubicin, camptothecin, and anti-inflammatory drug-  
4 curcumin, water-insoluble fluorophore-Nile red and congo red, and water-soluble  
5 fluorophore- Rose Bengal were successfully encapsulated in the hydroxyl functionalized  
6 nano-scaffold. Detail photophysical studies like absorption and emission were carried out to  
7 trace the fluorescence properties of the drug/dye loaded nano-scaffolds in the entire visible  
8 light region. *In vitro* drug release kinetics supported the enzymatic-degradation and enabled  
9 the delivery of cargoes exclusively at the intracellular compartments of the cancer cells. The  
10 cytotoxicity studies proved that the nascent polymers are non-toxic to cells whereas its drug-  
11 loaded nano-carriers accomplished more than 90 % killing in cervical cancer cell lines.  
12 Confocal microscopy studies confirmed the cellular uptake of the drug-loaded nano-carriers  
13 and depending upon the fluorescence properties of the dye/drug-loaded nano-systems the  
14 cancer cell bio-imaging could be accomplished in the entire visible region. The above  
15 investigation proved that the new hydroxyl functionalized polyester is very robust for  
16 accomplishing both therapeutics (by delivering drugs) and diagnostics (via fluorophores  
17 assisted bio-imaging) in L-amino acid bio-resource polymer nano-platform.  
18  
19  
20  
21  
22  
23  
24  
25  
26  
27  
28  
29  
30  
31

## 32 **Experimental Section**

33 **Materials:** L-Aspartic acid, 2,2- bishydroxymethyl propionic acid, dimethoxy propane, 1,12-  
34 dodecanediol, 1,8-octanediol, 1,10-decanediol, p-toulene sulphonic acid (pTSA), triethyl  
35 amine, N<sup>2</sup>- ethylcarboiimide hydrochloride, titanium tetrabutoxide (Ti(OBu)<sub>4</sub>),,  
36 hydrobenzotriazole, di-isopropyl ethyl amine, silicon wafers and pyrene were purchased from  
37 Sigma-Merck Cehmicals and used as it is. Chemicals for In-vitro Bio experiements: Horse  
38 liver esterase enzyme, porcine liver esterase,  $\alpha$ -chymotrypsin from bovine pancrease,  
39 doxorubicin HCl, curcumin, camptothecin, rose bengal, Nile red, congo red, tetrazolium salt:  
40 3-(4,5-dimethylthiazolyl)-2,5-diphenyltetrazolium bromide) MTT, glycerol, DAPI (4', 6-  
41 diamidino-2-phenylindole), Phalloidin–Tetramethylrhodamine B isothiocyanate,  
42 paraformaldehyde , were purchased from Sigma - Merck chemicals. Trypsin phosphate  
43 versene glucose (TPVG) solution was obtained from Hi-media. HeLa (Cervical cancer cells)  
44 and wild type mouse embryonic fibroblast (WT-MEF) were maintained in phenol red  
45 containing Gibco's DMEM medium (Dulbecco's modified eagle medium) with 1% (v/v)  
46 penicillin-streptomycin, 10% (v/v) fetal bovine serum (FBS). 96 and 6-well plastic plates  
47 with flat bottomed were obtained from Costar. Trypsin Phosphate Versene glucose was  
48 obtained from Himedia. Borosil glass based microslides were used for imaging, and  
49  
50  
51  
52  
53  
54  
55  
56  
57  
58  
59  
60

1  
2  
3 coverslips were obtained from corning and rinsed with ethanol and autoclaved prior to use.  
4 Nunc Lab Tek's 4 well Lab TEK cover glass chamber was used for live cell imaging.  
5 Lyotracker® Green DND-26 was bought from Cell Signalling Technologies (CST). Locally  
6 purchased chemicals: Solvents such as thionyl chloride, DMSO were purchased locally and  
7 used as it is. Methanol was purchased locally and dried and distilled prior to use. AR grade  
8 acetone and DCM were obtained from Finar Chemicals. HPLC THF and HPLC DMSO were  
9 obtained from spectrochem laboratories.  
10  
11  
12  
13  
14  
15  
16

**Methods:** <sup>1</sup>H and <sup>13</sup>C-NMR were recorded in 400 MHz and 600 MHz Bruker NMR  
17 spectrophotometer. High resolution mass spectrometry-electrospray ionization-quantitative  
18 time-of-flight liquid chromatography-mass spectrometry (HRMS-ESI-Q-TOF LC-MS,  
19 Waters). Mass of polymer aliquots were recorded using Applied Bio system 4800 PLUS  
20 matrix-assisted laser desorption/ionization (MALDI) TOF/TOF analyzer. Thermal  
21 gravimetric analysis (TGA) and differential scanning calorimetry (DSC) of polymers were  
22 carried out using PerkinElmer thermal analyzer STA 600 model and TA Q20 analyzer  
23 respectively. The heating rate and the cooling rate of 10°C/min were maintained during the  
24 data acquisition and indium standards were used to calibrate the system. Gel permeation  
25 chromatographic (GPC) plots were determined using Viscotek VE 1122 pump, Viscotek VE  
26 3580 RI detector, and UV/vis detector with polystyrene standards. For Dynamic light  
27 scattering (DLS) sizes of the nanoparticles, Malvern instrument with a Nano ZS-90 apparatus  
28 with inbuilt 633 nm red laser (90° angles) was used. The Atomic force microscopy (AFM)  
29 images were generated by VeecoNanoscope IV instrument in tapping mode. TEM samples  
30 were prepared by drop-casting the polymer nanoparticles aqueous solutions on sputter-coated  
31 holey carbon copper TEM grids. These dried samples were analyzed using Technai-300  
32 instrument. PerkinElmer Lambda 45 UV-vis spectrophotometer and SPEX Fluorolog  
33 HORIBA JOBIN VYON fluorescence spectrophotometer were used for all photophysics  
34 analysis of the loaded samples. MTT absorbance readings were recorded using varioskans  
35 FLASH instrument at 570 nm. Christ® Alpha 1-2 LD plus was employed to lyophilized  
36 frozen samples. The fixed cell and live cells images were procured using 405, 488, 561 nm  
37 lasers of LSM710 confocal microscope. WT-MEF cells live cell data was procured by  
38 multiphoton laser system (Verdi/Mira 900; Coherent) using the lasers 488 and 561 nm. The  
39 images were acquired using 40 X oil immersion objectives.  
40  
41  
42  
43  
44  
45  
46  
47  
48  
49  
50  
51  
52  
53  
54  
55  
56  
57  
58  
59  
60

**Synthesis of 2,2,5-trimethyl-1,3-dioxane-5-carboxylic acid (1):** This compound was synthesized following the reported procedure.<sup>(67)</sup> 2,2-Bishydroxymethyl propionic acid (10.0 g, 0.075 mol) and p-toluene sulfonic acid (p-TSA) (0.70 g, 0.004 mol) were taken in a two neck round bottom flask in dry acetone (100.0 mL). Dimethoxy propane (18.60 mL, 0.112 mol) was added dropwise to the above solution and the reaction mixture was stirred for 4 h at 25 °C. Triethylamine (2 drops) was added to neutralize the excess pTSA and the acetone was removed by rota-evaporation. The product was extracted in ethyl acetate. It was dried over anhydrous Na<sub>2</sub>SO<sub>4</sub> and the solvent was removed to get crystalline powder as product. Yield = 10.0 g (77 %). <sup>1</sup>H-NMR in CDCl<sub>3</sub> (400 MHz) δppm: 4.23- 4.20 (2H, d, -CH<sub>2</sub>), 3.72- 3.69 (2H, d, -CH<sub>2</sub>), 1.47- 1.44 (6H,d, -C(CH<sub>3</sub>)), 1.23 (3H, s, -C(CH<sub>3</sub>)). FTIR (cm<sup>-1</sup>): 3428, 2988, 2880, 1712, 1563, 1456, 1377, 1327, 1246, 1199, 1171, 1155, 1122, 1074, 1035, 988, 933, 903, 829, 761, 729, 716 and 666.

**Synthesis of dimethyl (2,2,5- trimethyl-1,3-dioxane-5-carbonyl) aspartate (2):** Amine salt of L-aspartic di-ester was synthesized as reported earlier.<sup>50,54</sup> Diisopropylethyl amine (26.5 mL, 0.15 mol) was added into the amine salt (10.0 g, 0.05 mol) in dry dichloromethane (DCM) (150.0 mL) and stirred at 25 °C until it dissolves completely. Hydroxybenzotriazole (6.86g, 0.050 mol), N'-ethylcarboiimide hydrochloride (8.6 g, 0.056 mol) and compound (1) (7.06 g, 0.040 mol) were added to the above solution and the reaction was carried out by stirring at 25 °C for 30 h. The DCM was rota-evaporated from the reaction mixture and crude product was extracted in ethyl acetate. The resultant product was purified using silica column in 30 % ethyl acetate in pet ether. The solvent was evaporated to get pale yellow liquid as a product. Yield =16.0 g (75 %). <sup>1</sup>H-NMR in CDCl<sub>3</sub> (400 MHz) δppm : 7.97 (bs, 1H, -NH), 4.83 (s, 1H, -CH), 3.88- 3.76 (dd, 2H, -CH<sub>2</sub>), 3.70- 3.76 (s, 5H, -CH<sub>2</sub> + -OCH<sub>3</sub>), 3.59 (s, 3H, -OCH<sub>3</sub>), 2.95- 2.78 (dd, 2H, -NH-CH<sub>2</sub>), 1.37 (s, 6H, -C(CH<sub>3</sub>)<sub>2</sub>), 0.91 (s, 3H, -C-CH<sub>3</sub>). <sup>13</sup>C-NMR in CDCl<sub>3</sub> (100 MHz): 174.7, 171.2, 98.5, 66.9, 52.6, 51.9, 48.6, 40.1, 36.3, 28.3, 18.4, and 17.6. FT-IR (cm<sup>-1</sup>): 3357, 2992, 2954, 2875, 1735, 1662, 1520, 1438, 1393, 1372, 1346, 1315, 1266, 1199, 1178, 1153, 1113, 1079, 1049, 1035, 993, 936, 915, 871, 826, 780, 749, 730 and 689.

**Synthesis of acetal-functionalized polyester:** Typical procedure for the polymerization reaction was explained for **P12A** polymer by melt condensation of monomer 2 with 1,12-dodecane diol. Monomer 2 (0.62 g, 1.89 mmol) and 1,12-dodecanediol (0.38 g, 1.89 mmol)

1  
2  
3 were taken in a melt polymerization tube and the mixture was melted at 100°C with constant  
4 N<sub>2</sub> purging.<sup>48,50</sup> Ti(OBu)<sub>4</sub> (1.0 mol %) was added as a catalyst to the melt and the tube was  
5 degassed at 0.01 mbar vacuum followed by purging with N<sub>2</sub> for five 5 minutes. The  
6 degassing and nitrogen purging was repeated 3 times. The polymerization was proceeded by  
7 stirring the melt to 150°C for 4h under a N<sub>2</sub> purge. During this process, methanol was  
8 removed along with the purge gas and the molten liquid gradually turned into a viscous mass.  
9 The polymerization was continued under a vacuum of 10<sup>-2</sup> mbar for 2 h to produce polymer.  
10 Yield= 0.80 g (95 %). <sup>1</sup>H-NMR (400 MHz, CDCl<sub>3</sub>) δ ppm: 8.04 (s, 1H, -NH), 4.91 (m, 1H, -  
11 CH), 4.17 (t, 2H, -COOCH<sub>2</sub>), 4.09 (t, 2H, -NHCOOCH<sub>2</sub>), 3.96 (d, 1H, -CH<sub>2</sub>), 3.88 (d, 1H, -  
12 CH<sub>2</sub>), 3.77 (d, 2H, -CH<sub>2</sub>), 3.06-2.87 (m, 2H, -CH-CH<sub>2</sub>), 1.64 (m, 4H, -COOCH<sub>2</sub>CH<sub>2</sub>), 1.48  
13 (s, 6H, -C(CH<sub>3</sub>)<sub>2</sub>), 1.26 (bs, 16 H, -aliphatic protons), 1.02 (s, 3H, -CH<sub>3</sub>). <sup>13</sup>C-NMR (100  
14 MHz, CDCl<sub>3</sub>) δ ppm: 174.1, 171.7, 97.8, 66.9, 65.8, 64.6, 48.3, 39.9, 36.4, 29.4, 28.4, 24.8,  
15 18.1, and 17.7. FT-IR (cm<sup>-1</sup>): 3324, 2926, 2855, 1733, 1646, 1530, 1461, 1396, 1350, 1187,  
16 1046, 992 and 911.

17  
18  
19 A similar procedure was followed for the polycondensation of monomer 2 with 1,10-  
20 decanediol and 1,8-octanediol to yield polymers P10A and P8A, respectively, and these  
21 details are given in the supporting information.  
22  
23  
24  
25  
26  
27  
28  
29  
30  
31  
32  
33

34  
35 **Synthesis of hydroxyl-functionalized polyester:** The de-protection procedure was explained  
36 in detail for polymer P12H. The polymer P12A (0.46 mg, 1.0 mmol) was taken in a round  
37 bottom flask and dissolved in dichloromethane (DCM) (4.0 mL). Trifluoroacetic acid (0.78  
38 mL, 10.0 mmol), and water (0.80 mL) were added under ice-cold conditions, brought to 25  
39 °C, and the stirring was continued for 2 h. The excess solvent was removed from the reaction  
40 mixture using rota-evaporator. The polymer was obtained as a viscous solid mass. Yield=  
41 0.39 g (94 %) <sup>1</sup>H-NMR (400 MHz, CDCl<sub>3</sub>) δ ppm: 8.04 (s, 1H, -NH), 4.91 (m, 1H, -CH),  
42 4.17 (t, 2H, -COOCH<sub>2</sub>), 4.09 (t, 2H, -NHCOOCH<sub>2</sub>), 3.96 (d, 1H, -CH<sub>2</sub>), 3.88 (d, 1H, -CH<sub>2</sub>),  
43 3.77 (d, 2H, -CH<sub>2</sub>), 3.06-2.87 (m, 2H, -CH-CH<sub>2</sub>), 1.64 (m, 4H, -COOCH<sub>2</sub>CH<sub>2</sub>), 1.48 (s, 6H, -  
44 C(CH<sub>3</sub>)<sub>2</sub>), 1.26 (bs, 16 H, -aliphatic protons), 1.02 (s, 3H, -CH<sub>3</sub>). <sup>13</sup>C-NMR (150 MHz,  
45 CDCl<sub>3</sub>) δ ppm: 176.7, 171.4, 171.3, 70.7, 68.9, 68.4, 66.5, 65.7, 63.3, 53.8, 48.9, 48.1, 47.2,  
46 45.9, 42.2, 41.1, 36.2, 35.9, 32.9, 32.7, 29.8, 29.7, 29.6, 29.6, 29.5, 29.4, 29.3, 28.64, 28.6,  
47 26.0, 25.9, and 25.8. FT-IR (cm<sup>-1</sup>): 3332, 2926, 2654, 1735, 1649, 1533, 1460, 1396, 1350,  
48 1281, 1199, 1051, 999, 921, 629 and 608.  
49  
50  
51  
52  
53  
54  
55  
56  
57  
58  
59  
60

1  
2  
3 A similar procedure was followed for the de-protection of P10A and P8A to yield  
4 hydroxyl polymers P10H and P8H, respectively, and these details are given in the supporting  
5 information.  
6  
7  
8  
9

10 **Self-assembly and Encapsulation Studies:** The self-assembly of hydroxyl functionalized  
11 polyesters were carried out using the dialysis method explained. About 5.0 mg of the polymer  
12 sample was dissolved in 2.0 mL of DMSO+water (2/3 v/v) and the solution was dialyzed  
13 against water using the semi-permeable membrane of MWCO 1000 Da for more than 48 h.  
14 During this process, freshwater was replenished regularly in the reservoir to remove DMSO.  
15 For loading of drugs, for example doxorubicin loading, 5.0 mg of polymer 0.5 mg  
16 doxorubicin HCl were used. Prior to use doxorubicin HCl was neutralized using tri-ethyl  
17 amine. The dialysis using semi-permeable dialysis membranes of cut off of 1.0 kD ensured  
18 the removal of the un-encapsulated drug molecules. The resultant dialyzed solutions were  
19 filtered, lyophilized and stored at 4°C. The lyophilized nanoparticles were re-dispersed in  
20 media prior to use. A similar protocol was followed for the encapsulation of curcumin  
21 (CUR), Camptothecin (CPT), Nile red (NR), Rose Bengal (RB) and Congo Red (CR). For  
22 loading of NR, 100.0 µg was taken as their feed for loading. For photo-physical experiments  
23 and DLS measurements, the dialyzed filtered solutions were used as it is. DLC (Drug  
24 Loading Content) and DLE (Drug Loading Efficiencies) were measured using the equations  
25 (1) and (2) as mentioned below:<sup>50,54</sup>  
26  
27  
28  
29  
30  
31  
32  
33  
34  
35  
36  
37

$$38 \text{ Drug/Dye Loading Content (DLC, in \%)} = \frac{\text{weight of loaded drug OR dye}}{\text{weight of polymer}} \times 100 \dots\dots\dots(1)$$

$$39 \text{ Dye/ Dye Loading Efficiency (DLE, in \%)} = \frac{\text{weight of loaded drug OR dye}}{\text{Total weight of drug OR dye fed}} \times 100 \dots\dots\dots(2)$$

40  
41  
42  
43 For HR-TEM, AFM images 0.1 mg/mL freshly dialyzed samples were used. The  
44 samples were sonicated for ten minutes prior to drop-casting. Critical aggregation  
45 concentration of the polymer sample was determined using pyrene as a fluorescence probe for  
46 various concentrations of polymer nanoparticles and the procedure has been adopted from the  
47 details from our earlier reports.<sup>51</sup>  
48  
49  
50  
51  
52  
53

54 **Enzymatic-biodegradation Studies:** The biodegradation studies were carried out by taking  
55 the P12H-DOX nanoparticles in a dialysis tube of 1kD cut off and placed in a beaker  
56 containing PBS buffer. The concentration of DOX was taken as 80.0 µg in the total solution.  
57 The solution was incubated at 37 °C and the absorbance of the solution outside the dialysis  
58  
59  
60

1  
2  
3 membrane was measured at fixed time intervals. To mimic the lysosomal conditions, the  
4 same set up was used, with an additional 10 U of horse liver esterase enzyme,  $\alpha$ -chemotrysin  
5 from bovine pancreas, porcine liver esterase enzyme and acidic pH 4.0, to study the stability  
6 of these nanoparticles . The absorbance of the solution in the reservoir was measured and the  
7 relative amount of Doxorubicin w.r.t the total initial DOX concentration was plotted against  
8 time as the release profile of the nanoparticles.  
9  
10  
11  
12  
13  
14

15 **Photophysical studies:** The drugs DOX, CPT, and CUR, as well as the dyes NR, RB, and  
16 CR, were loaded in the P12H nanoparticles and were subjected to absorbance and  
17 fluorescence studies to determine the photophysical characteristics of the polymer loaded  
18 nanoparticles. The fluorescence of the drugs and dyes were measured at their respective  
19 absorbance maxima, keeping the slit width 2nm for all the measurements.  
20  
21  
22  
23  
24  
25

26 **Cytotoxicity Studies:** Cytotoxicity study was done following our earlier reported procedure  
27 by MTT-assay.<sup>50,55</sup> This colorimetry assay was employed to determine the presence of living  
28 or metabolically active cells in the system. The ability of NAD(P)H assisted cellular  
29 oxidoreductase enzyme to reduce the 3-(4,5-dimethylthiazol-2-yl)-2,5- phenyl tetrazolium  
30 bromide (MTT) to purple formazan crystals was employed to determine the number of living  
31 cells present in the system after exposure to the polymers and polymer loaded samples for 48  
32 h. HeLa cell lines ( cancerous) and WT-MEF (Wild type mouse embryonic fibroblast) cell  
33 lines (normal healthy cells) were chosen for this purpose and 1000 cells in each well in a 96  
34 well plate and grown for 24h in a 5 % CO<sub>2</sub> incubator at 37 °C. Various concentrations of  
35 P12H-DOX nanoparticles were added and the cells were incubated for 48 h. A control of  
36 viable cells was also maintained and all these experiments were carried out in triplicates. After  
37 48 h and experiment completion, the media was aspirated, followed by addition of 100  $\mu$ L of a  
38 freshly prepared MTT solution (50.0  $\mu$ g /mL in DMEM) was added to each well. The treated  
39 cells were further incubated for 4 h at 37 °C under a CO<sub>2</sub> environment. The formazan crystal  
40 obtained precipitated out at the bottom of the flat plate due to their insolubility in media. The  
41 media was carefully removed and replaced with 100  $\mu$ L of HPLC DMSO. The plate was  
42 shaken gently to dissolve the crystals. The photometric absorbance of this purple solution was  
43 collected at 570 nm and average of the three absorbance intensity was used for calculations.  
44 The control cells (without any polymer or samples) were set as standard and the numbers of  
45 metabolically active cells (viable cells) were calculated with respect to these numbers of cells.  
46  
47  
48  
49  
50  
51  
52  
53  
54  
55  
56  
57  
58  
59  
60

1  
2  
3 Out of three, if any value was out of standard deviation, then it was omitted during the  
4 calculations. Cell viability percentage was plotted against the concentration of the polymers.  
5 The MTT assays in WT-MEF (Wild type mouse embryonic fibroblast) were carried out for  
6 72h following the same procedure.  
7  
8  
9

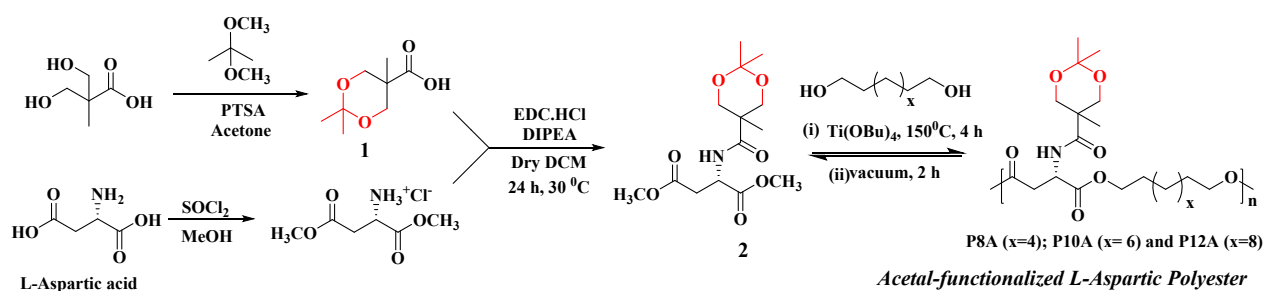
10  
11 **Confocal Imaging:** This study was done following our earlier reported procedure.<sup>50-52, 54-55</sup>  
12 Cornings coverslips were thoroughly washed with 70% ethanol, flame dried and autoclaved  
13 and used for the growing cells. One coverslip each was placed in a 6-well plate and was  
14 washed once with 1.0 mL PBS and media. HeLa cells (passage number 40 and 41 were used  
15 for these experiments).  $1 \times 10^5$  HeLa cells were seeded in each well in 2.0 mL media and  
16 were grown for 24h under a CO<sub>2</sub> environment at 37 °C. For bio-imaging applications, freshly  
17 dialyzed P12H nanoparticles (loaded with drugs and dyes) were lyophilized for 24 h and were  
18 re-dispersed in media. Concentration of drugs and dyes were taken as 5.0 – 20.0 μM. Cells  
19 were incubated for 5 h and then washed with PBS (1.0 mL) twice to remove all the traces of  
20 the media or suspended fluorophores and drugs that were not taken up by the cells. Cells were  
21 fixed using 4% paraformaldehyde (PFA) solution (in PBS) and stained with DAPI for 2  
22 minutes (for DOX) and were fixed on clean glass slides using mounting media for cell  
23 imaging. In fixed cell imaging for P12H-DOX the cellular distribution was monitored using  
24 phalloidin green to stain the actin filaments of the cells green. The cells were imaged on  
25 confocal microscopy and the DAPI was used for staining nuclei of the cells. The phalloidin  
26 was imaged using 488 nm laser and emission was collected in green channel. DAPI and CPT  
27 were excited at 405 nm laser, and emission was collected at 415- 600 nm (blue channel).  
28 Laser power, gain and airy units for DAPI were 2, 669, and 1.0 A. U, and for CPT was 12,  
29 837, 1.0 A.U. respectively. DOX and CR chromophore was excited at 488 nm and its  
30 emission was collected at 535- 797 nm (red channel), with laser power 3.0, gain 960 and 1.0  
31 A.U. NR and RB were excited at 514 and 561 laser respectively and emission was collected at  
32 red channels. The confocal images were processed in image J software and were processed  
33 using windows and levels in the software. Three regions of interests were selected in the  
34 similar-looking cells and in the background and the corrected total cell fluorescence (CTCF)  
35 calculated following:  $CTCF = \text{Integrated Density} - \text{Mean of the background} \times \text{area of the cell}$ .  
36 The average of the three values and standard deviations were calculated, and this differential  
37 uptake of the cells was plotted.  
38  
39  
40  
41  
42  
43  
44  
45  
46  
47  
48  
49  
50  
51  
52  
53  
54  
55  
56  
57  
58  
59  
60

1  
2  
3 **Lysosomal Tracking experiments:** A chamber was employed to carry out live-cell imaging  
4 experiments.<sup>54</sup> 25000 HeLa cells with passage number 40 were seeded a 4 well live-cell  
5 chamber and 300.0  $\mu$ L media was added and the cells were grown by incubation as mentioned  
6 for cellular imaging for 24h. P12H-DOX nanoparticles were subjected to the cells keeping the  
7 concentration of DOX fixed at 20.0  $\mu$ M for each experiment. The nanoparticles were added at  
8 different time points to the independent wells at time 5, 15, 60 and 600 min. Free DOX at the  
9 same concentration was also incubated with the cells as a control. After the experiment  
10 completion, the media containing the suspended nanoparticles were aspirated and 300.0  $\mu$ L of  
11 freshly prepared solution of LysoTracker Green DND-26 (0.15  $\mu$ L in 3.0 mL media) was  
12 added to each well and the chamber imaged. The LysoTracker Green DND-26 was excited by  
13 laser 488nm and DOX was excited by 561 nm laser and images were collected at green and  
14 red channel respectively. Similar experiments were carried out for WT-MEF cells (passage  
15 21-22). The images thus obtained were processed in Image J software using the windows and  
16 levels tool and were plotted. The CTCF (corrected total cell fluorescence) plots were  
17 generated using Image J software for 8-bit images and a set of 3; three regions of interests  
18 were chosen from the images to calculate the intensity.  
19  
20  
21  
22  
23  
24  
25  
26  
27  
28  
29  
30  
31  
32  
33  
34  
35  
36  
37  
38  
39  
40  
41  
42  
43  
44  
45  
46  
47  
48  
49  
50  
51  
52  
53  
54  
55  
56  
57  
58  
59  
60

## Results and Discussion

### *Synthesis of Hydroxyl Functionalized Polyesters*

L-Aspartic acid bio-resource was selected to make the new classes of hydroxyl functionalized polyesters by melt polycondensation route as shown in Scheme-1. The hydroxyl groups in 2,2-bishydroxymethyl propionic acid was reacted with dimethoxypropane to make cyclic-acetal molecule (**1**). The reaction of compound **1** with the amine salt of the L-aspartic di-ester yielded the multifunctional monomer (**2**) and its structure was confirmed by NMR spectroscopy in Figure S1. The thermogravimetric analysis proved that the monomer has very good thermal-stability up to 200 °C and confirmed its suitability for melt polycondensation reaction (Figure S1). Three commercial diols 1,12-dodecanol, 1,10-decane diol, and 1,8-octane diol were chosen and Ti(OBu)<sub>4</sub> (1 mole %) was employed as a catalyst for the transesterification polycondensation process. The di-carboxylic esters in the monomer reacted with diols to yield aliphatic ester chemical linkages under the melt transesterification process while the amide and acetal functional units in the pendants were inert during this process. The polymerization was carried out first under nitrogen purge for 4 h at 150 °C and then under vacuum (0.01 mbar) to produce polymers. The resultant aliphatic polyesters have one cyclic-acetal functional group in each repeating unit and these polymers are referred to as **P12A**, **P10A**, and **P8A** with respect to the number of carbon atoms in the diol segment and “A” for acetal groups (see Scheme-1).



**Scheme 1.** Synthesis of acetal functionalized polyesters from L-aspartic acid.

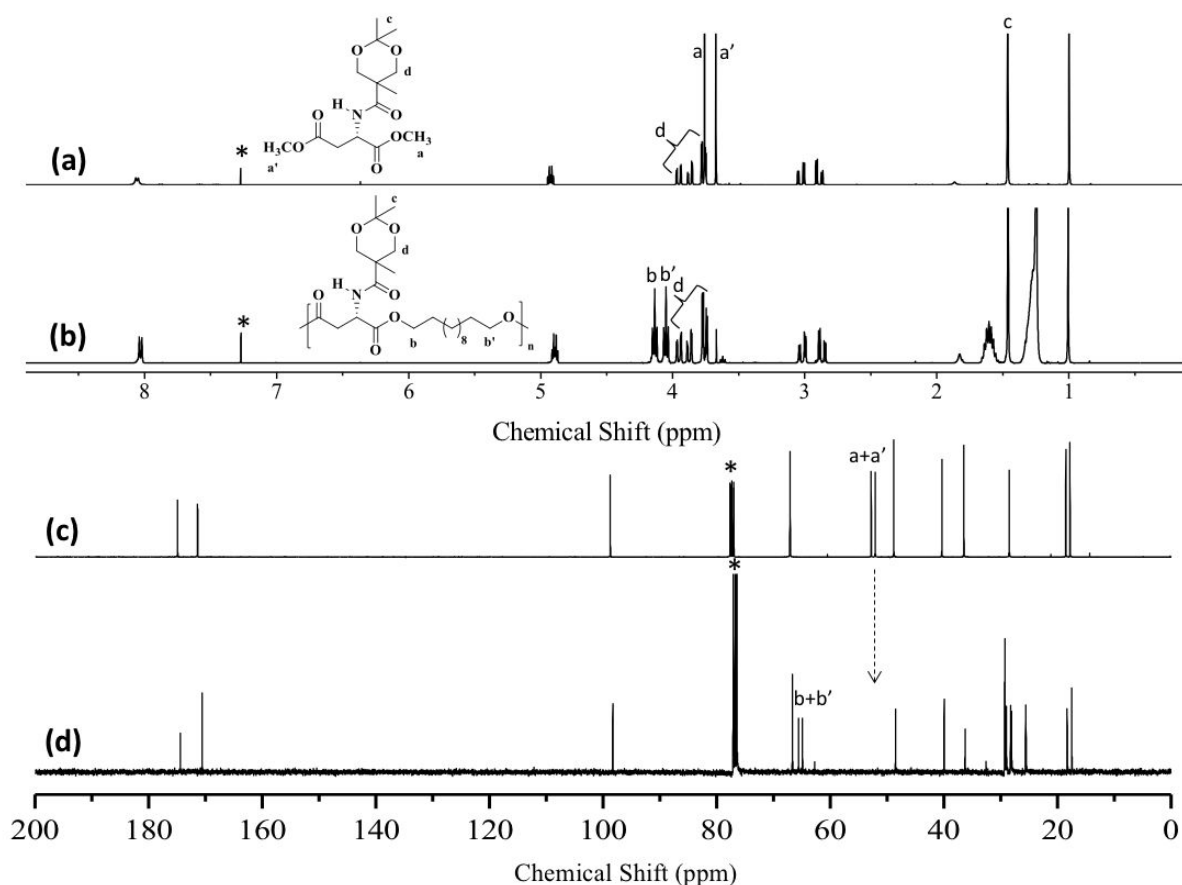


**Figure 2.** NMR spectra of monomer (a and c) and polymer P12A (b and d) were recorded in  $CDCl_3$ . The different atoms are assigned by alphabets and the solvent peaks are indicated by asterisks.

The  $^1H$ -NMR spectrum of the monomer and the polymer **P12A** are given in Figure 2 and the different types of protons and carbons are assigned by alphabets. The methyl ester peaks in the monomer at 3.67 and 3.59 ppm (peak a and a' in Figure 2a) diminished and new ester peaks with respect to the formation of polymer chains  $RCOOCH_2CH_2$  appeared at 4.17 and 4.09 ppm (peaks b and b' in Figure 2b). The acetal group  $-CCH_2OC(CH_3)_2$  at 1.48 ppm (peak c) and multiple peaks at the region of 3.9 to 3.6 ppm with respect to  $-CCH_2OC(CH_3)_2$  (peak d) were found to be completely intact in both monomer and polymer spectra. This observation confirmed that the acetal unit was completely inert and it was not disturbed during the melt polycondensation reaction. The comparison of ratios of intensity of new ester peaks  $RCOOCH_2CH_2$  (peaks at 4.17-4.09 ppm, b and b') with that of the methyl esters at the chain ends (peaks at 3.67-3.59 ppm) in the polymer spectrum enabled the determination of the number average repeating units ( $X_n$ ) in the polymer chains. The  $X_n$  was determined as 30-32 in P12A and the substitution of this value in Carothers equation [ $X_n = 1/(1-p)$ ] gave the % of reaction,  $p > 98$  %. The occurrence of the polycondensation process was further supported

by  $^{13}\text{C}$ -NMR (Figures 2c and 2d). The peaks of major importance were the methyl ester carbon peaks at 52.6 and 51.9 ppm in the monomer (Figure 2c) which completely disappeared and new ester carbon peaks appeared in the polymer spectrum at 65.7 and 65.0 ppm (see Figure 2d). Interestingly the acetal carbon atoms  $-\text{CCH}_2\text{OC}(\text{CH}_3)_2$  and  $-\text{CCH}_2\text{OC}(\text{CH}_3)_2$  at 98.5 ppm and 17.7, respectively, in the polymer and monomer spectra were not disturbed. Based on the above analysis, it may be concluded that (i) the multifunctional L-aspartic acid monomer 2 was stable under melt condition to condense with commercial diols to produce linear acetal-containing polyesters. Similarly, the structures of the polymers P10A and P8A were confirmed by NMR and the details are given in Figure S2. The molecular weights of the polymers were determined by GPC in tetrahydrofuran solvent and their respective chromatograms are shown in Figure 3a and the molecular weights were summarized in the table in Figure 3b. The P12A acetal-polymer showed the formation of high molecular weights as  $M_n = 12 \times 10^3$  g/mol and  $M_w = 25 \times 10^3$  g/mol with a polydispersity of 2.3. The P10A and P8A polymers showed the formation of moderate molecular weights in the range of  $M_n = 5 \times 10^3$  g/mol and  $M_w = 18 \times 10^3$  g/mol.

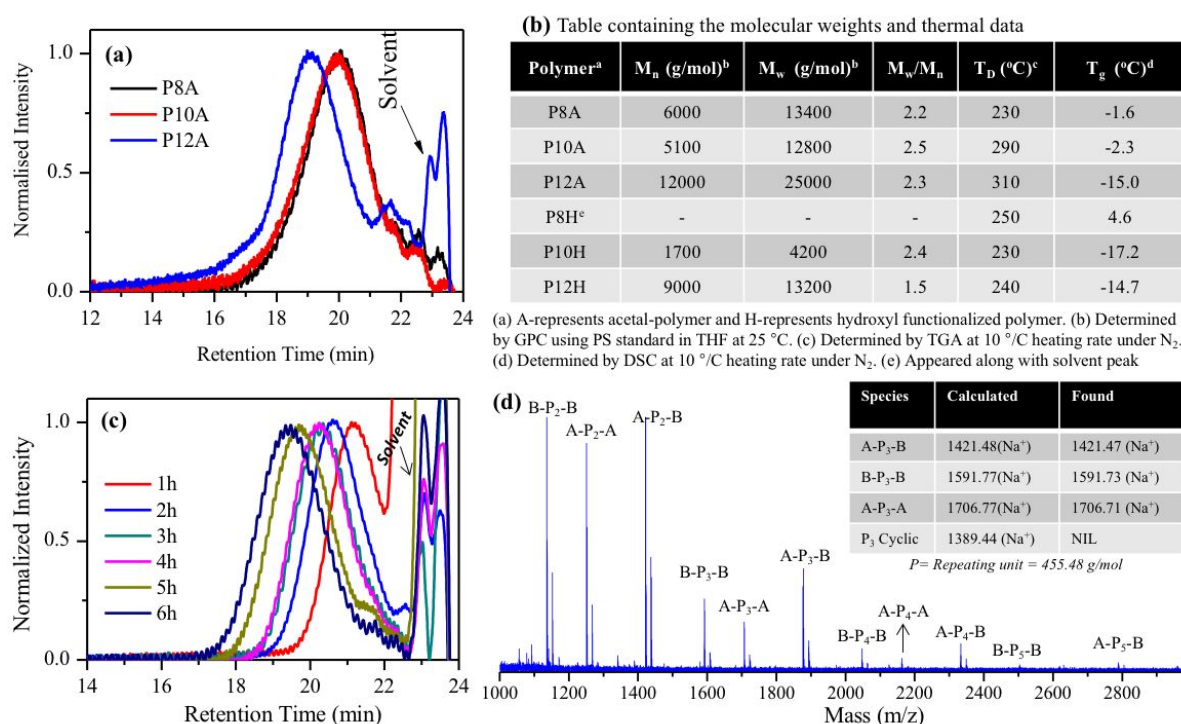
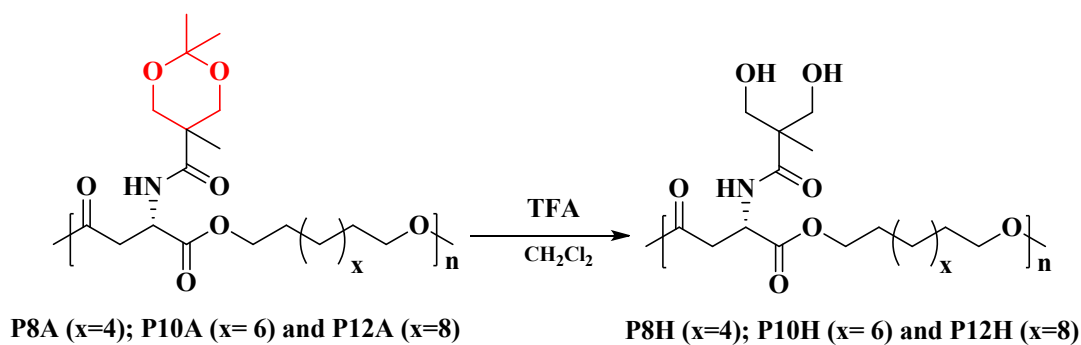


**Figure 3.** (a) GPC chromatograms of acetal functionalized polyesters in tetrahydrofuran at 25 °C. (b) GPC molecular weights and thermal properties of the polymers are shown in the table. (c) GPC chromatograms of polymer P12A aliquots taken at various time intervals. (d) MALDI-TOF mass spectrum of P12A aliquots taken at 2 h. The inset table shows the calculated and found mass peaks for different types of chain ends for trimer species.

1  
2  
3  
4  
5 To further study the molecular weight build-up in the polycondensation reaction;  
6 polymerization kinetic was carried out for the P12A polymer synthesis. Polymer sample  
7 aliquots were taken at regular time interval and they were subjected to NMR and GPC  
8 analysis. The GPC plot of the aliquots in Figure 3c revealed the formation of higher  
9 molecular weight chains with an increase in reaction time. The GPC plots gradually changed  
10 from multi-modal to narrow disperse samples as a result of the transformation from  
11 oligomers to high molecular weight polymer chains in the condensation process. The NMR  
12 spectra of the aliquots in Figure S3 showed the disappearance of the methoxy protons and  
13 appearance of the new ester peaks as observed in Figure 2. The plot of  $M_n$  versus %  
14 conversion showed typical trend for condensation polymerization with respect to increase in  
15 the molecular weight at higher % conversion (see Figure S4). The polydispersity of the  
16 aliquots were found to be  $\sim 2.0$  which is typically expected for condensation polymers. To  
17 study the non-interference of the acetal units during the polycondensation process, the  
18 aliquots were subjected to MALDI-TOF MS analysis for end group analysis. A MALDI-TOF  
19 spectrum for 2h aliquot is shown in Figure 3d and the peaks are assigned for different types  
20 of chain ends (for MALDI-TOF spectra of other aliquots, see Figure S5). In a typical A-A +  
21 B-B polycondensation, the growing chains are expected to have four types of reactive species  
22 such as A- $P_n$ -A, A- $P_n$ -B, B- $P_n$ -B and  $P_n$ -cyclic, where  $P_n$  represents the repeating unit of 'n<sup>th</sup>'  
23 chain. In the present case, each repeating unit mass is corresponding to 455.48 g/mol; thus,  
24 for the trimer species, the mass for the different types of chain ends are calculated and shown  
25 in the table inset. The peaks in the MALDI-TOF spectrum are assigned with respect to these  
26 chains showed in Figure 3d. Two important points are clear from these studies; (i) the peaks  
27 in the MALDI-TOF spectrum preferably matched with the expected repeating unit mass  
28 having protected acetal chemical linkages, and (ii) there are no traces of the peaks with  
29 respect to the macro-cyclic ( $P_n$ ) formation. These observations confirmed that the acetal units  
30 were stable under melt polycondensation process and also the polymerization preferably  
31 underwent via linear chain formation to produce higher molecular weight chains. This  
32 revealed that the melt transesterification process applied for L-aspartic acid monomer is  
33 stable to produce the acetal-functionalized polyesters under solvent-free process.  
34  
35  
36  
37  
38  
39  
40  
41  
42  
43  
44  
45  
46  
47  
48  
49  
50  
51  
52  
53  
54  
55  
56  
57  
58  
59  
60



**Scheme 2:** Synthesis of hydroxyl functionalized *L*-aspartic acid based polyesters.

The de-protection of the above acetal-polyesters yielded their corresponding hydroxyl functionalized polyesters **P12H**, **P10H**, and **P8H** (H-hydroxyl) (see Scheme-2). For this purpose, the acetal-polymers were subjected to de-protection under acidic medium (using trifluoroacetic acid, TFA) to yield the hydroxyl functionalized polyesters as shown in Scheme-2. The complete de-protection of the acetal units without affecting the polyester backbone was confirmed by NMR spectroscopy analysis. <sup>1</sup>H-NMR spectra of the hydroxyl functionalized polymers are shown in Figure S6. The polymer spectra showed the disappearance of the acetal units (vanishing of peak c at 1.48 ppm) and appearance of the new hydroxyl units R-CH<sub>2</sub>OH at 3.8-3.5 ppm in the polymer (see Figure S6). Further, the comparisons of the peak intensities in the hydroxyl polyester in Figure S6 with respect to the ester peaks RCOOCH<sub>2</sub>CH<sub>2</sub> (peaks at 4.11-4.19 ppm) and hydroxyl units R-CH<sub>2</sub>OH at 3.8-3.6 ppm matched very well with 1:1 ratio for the expected polymer structure. The de-protected polymer sample was subjected to HRMS analysis and the data is shown in the supporting information Figure S7. The deprotected polymer samples showed peaks with respect to the expected hydroxyl functionalized polymer structure. The peaks corresponding to the A-P<sub>n</sub>-B and B-P<sub>n</sub>-B where n= 1-3 were clearly visible which further supported the complete de-protection of acetal to hydroxyl functional groups. This confirmed that the de-protection was accomplished without affecting the aliphatic polyester backbone. GPC molecular weights of the hydroxyl functionalized polymers were determined by GPC and their plots are shown in Figure S8 and the molecular weights are summarized in Table 3b. The hydroxyl functionalized polymer exhibited higher retention time compared to its acetal-polymer and this trend was attributed to the variation in the hydrodynamic volume of these two different polymer structures in tetrahydrofuran (GPC solvent). The GPC plots of P12H and P10H could be clearly visualized whereas the P8H polymer eluted along with the solvent (see figure

1  
2  
3 S8). The thermal properties of the polymers were studied by TGA and DSC, and the data are  
4 shown in Figure S9 and S10. The thermal stability of the acetal-polymers was found to be  
5 very good in the range of 290-310 °C whereas their hydroxyl functionalized polymers  
6 showed stability only up to 240-250 °C. The relatively less thermal stability of the hydroxyl  
7 functional polyesters are not clearly understood at present and it may be partially attributed to  
8 thermal hydrolysis of aliphatic ester backbone by the back-biting of hydroxyl groups.  
9 Nevertheless, this is not a limitation on the hydroxyl polymers for biomedical applications  
10 since they have stability up to 250 °C which is sufficient enough for drug delivery  
11 application. DSC thermograms of the polymers showed only glass transition temperature ( $T_g$ )  
12 with respect to amorphous polymers. The  $T_g$  of the acetal-polymers were found to be -15 to -  
13 2 °C whereas the hydroxyl polymers showed slightly higher  $T_g$  in the ranges of 4 to 6 °C. The  
14 higher  $T_g$  values for the hydroxyl polymers is attributed to the possibility for the existence of  
15 hydrogen bonding interactions among the hydroxyl functional groups at the periphery. Based  
16 on the above analysis, it may be summarized: (i) the melt transesterification underwent more  
17 than 98 % to produce high molecular weight chains, and (ii) the de-protection of the acetal-  
18 polymers yielded new classes of hydroxyl-functionalized polyesters, for the first time, from  
19 L-aspartic acid in the literature. Hence, the new synthetic strategy is very good to produce  
20 new classes of well-defined acetal-containing and hydroxyl functionalized aliphatic  
21 polyesters from L-amino acid bio-resources. Among all three polymers, the hydroxyl  
22 functionalized polymer synthesized using 1,12-dodecanediol possessed higher molecular  
23 weights; thus, the polymer P12H was further chosen to demonstrate the biomedical  
24 application of these newly designed structures in drug delivery to cancer cells.  
25  
26  
27  
28  
29  
30  
31  
32  
33  
34  
35  
36  
37  
38  
39  
40  
41  
42  
43  
44  
45  
46  
47  
48  
49  
50  
51  
52  
53  
54  
55  
56  
57  
58  
59  
60

### ***Self-assembly and Drug Encapsulation***

The L- aspartic acid based hydroxyl functionalized polymers have unique structural geometry with hydrophobic polyester backbone and bis-hydroxyl groups in every repeating unit providing hydrophilic at periphery. As a result, the polymer structures gain appropriate amphiphilicity to self-assemble in the aqueous medium. The side chain part having the hydroxyl units tends to phase segregate away from the hydrophobic backbone; thus it produces hair-pin bend type amphiphiles in the aqueous medium. The subsequent aggregation of these amphiphiles self-assembled into polymer nanoparticles with hydrophobic core and hydroxyl groups containing periphery as shown in Figure 4a. To produce the self-assembled nano-assemblies typically the hydroxyl polymers were dissolved in DMSO+water (2:3 v/v) solvent mixture and dialyzed using semi-permeable membrane having MWCO of 3500 Da. The reservoir was replenished periodically with fresh water and this facilitates the complete removal of the DMSO and other impurities. At the end of the dialysis clear solution was obtained which was lyophilized and the sample was stored at 4 °C. To study the encapsulation capabilities of the polymer nano-assemblies, a similar dialysis procedure was followed in which the desired drugs or fluorophore dyes were also taken along with the polymer. The un-encapsulated drugs or dye molecules were removed continuously by replenishing with fresh water in the reservoir until otherwise the solution became colorless (at least for 48 h). Two clinically important anticancer drugs doxorubicin (DOX) and camptothecin (CPT), and anti-inflammatory natural drug curcumin (CUR) were chosen. Three fluorophore dyes (or markers) Nile red (NR), Rose Bengal (RB) and Congo Red CR) employed routinely for bio-imaging application were also chosen for encapsulation. It is important to mention that DOX and RB are water-soluble whereas all other four molecules (CUR, CPT, NR, and CR) are water-insoluble. Hence, the selections of these drugs/dyes provide appropriate choice to check the encapsulation capabilities of the newly designed hydroxyl functionalized polyester P12H. The P12H encapsulated nanoparticles are referred to as P12H-DOX, P12H-CPT, P12H-CUR, P12H-NR, P12H-RB, and P12H-CR. The dialyzed polymer solution containing these drugs and dyes in the vial was shown in Figure 4a.

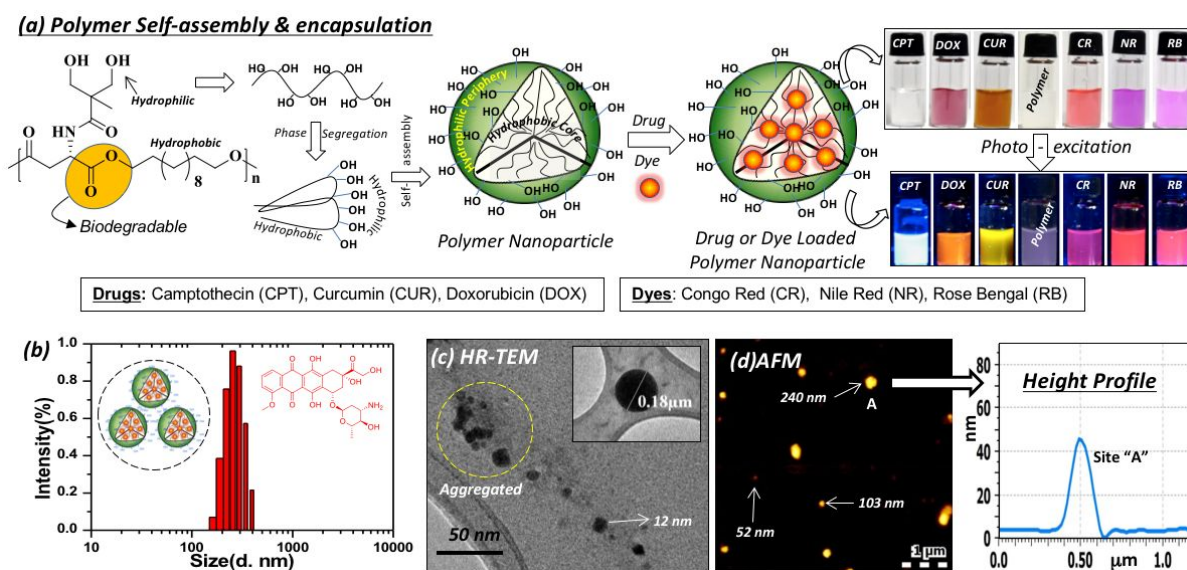


**Figure 4:** (a) Schematic representation of self-assembly of hydroxyl functionalized L-aspartic acid nanoparticles and their drug or dye loading capabilities. The photographs showing the DOX, CPT, CUR, NR, CR, and RB encapsulated vials along with nascent polymer under normal light and upon photo-excitation. (b) DLS histograms of DOX loaded nanoparticles P12H-DOX and the schematic representation of aggregated nanoparticles. (c) High-resolution transmission electron microscope images of P12H-DOX. The figure in the inset shows the HR-TEM image of the aggregated polymer nanoparticles. (d) Atomic force microscopy image of P12H-DOX and the height profile of the nanoparticles.

The aqueous solution nano-aggregates of the P12H were studied by dynamic light scattering (DLS) and the DLS histogram of P12H-DOX is shown in Figure 4b. DLS studies showed that P12H-DOX exhibited mono-modal histogram with size  $255 \pm 40$  nm. The PDI of the P12H-NR, P12H-CR, P12H-CUR, P12H-RB, P12H-DOX, P12H-CPT and P12H nanoparticles were found to be in the range of 0.12 to 0.30. The DOX loaded nanoparticles were further subjected to high-resolution transmission electron microscope imaging and the TEM image in Figure 4c showed the formation of 25-30 nm nanoparticles and their subsequent aggregation into large nanoparticles of 180 nm. High resolution TEM images clearly showed the co-existence of the aggregation of many nanoparticles together to produce larger size aggregated nanoparticles of 180 nm in size. During the self-assembly process, the amphiphilic polymer chains collapsed into coil-like form which typically undergoes aggregation to produce individual nano-particles of typically 15-20 nm in size. These nanoparticles further undergo aggregation to produce larger nanoparticles of 180 nm in size (shown as inset in Figure 4c). The hydroxyl substituted polymers reported here has clear

1  
2  
3 hydrophilic (hydroxyl units) and hydrophobic (back bone) domains within their structure,  
4 thus the phase separation facilitated the observation of both individual nanoparticles and their  
5 aggregation together into exhibiting larger nanoparticle size formation (shown by circle) in  
6 the TEM image in Figure 4c. Additional TEM images are given in the supporting information  
7 Figure S11 to support this aggregated nanoparticle formation. DLS histograms typically  
8 showed the hydrodynamic diameter of the aggregated nanoparticles in the aqueous medium;  
9 thus, these nano-aggregated assemblies matched with the aggregated nanoparticles in HR-  
10 TEM image. Atomic force microscope (AFM) is a relatively soft technique to measure the  
11 size of the nano-aggregates which are directly drop casted on the mica surface. AFM image  
12 in Figure 4d of the P-12H-DOX showed the existence of smaller (50 nm) as well as larger  
13 nanoparticles (220 nm). The above analysis suggested that the hydroxyl polyester P12H  
14 nanoparticles self-assembled into smaller nano-assemblies which underwent aggregation to  
15 produce nearly 200 nm nanoparticles. The height and width of the nanoparticles measured by  
16 AFM is showed along with Figure 4d. The half-width at maximum showed the size of the  
17 nanoparticle as 200 nm and supported the size of the nanoparticle measured in HR-TEM and  
18 DLS. DLS histograms of other drug-loaded and fluorophore loaded nanoparticles are shown  
19 in the supporting information in Figure S12. These drug or dye loaded nanoparticles showed  
20 the average sizes < 250 nm and matched with the DLS and TEM observation of P12H-DOX  
21 sample. The critical aggregate concentration (CAC) of the polymer was determined using  
22 pyrene as chromophores following the literature report.<sup>51</sup> Typically 0.6  $\mu\text{M}$  concentration of  
23 pyrene was employed for the CAC studies by varying the polymer concentration ranging  
24 from  $1 \times 10^{-1}$  to  $1 \times 10^{-7}$  mg/mL. The  $I_1/I_3$  ratio of the emission peak intensities in pyrene was  
25 plotted against the concentration of the polymer for the CAC determination (see Figure S13).  
26 The break point was observed at  $0.53 \times 10^{-6}$  g/mL with respect to the CAC of the newly  
27 designed hydroxyl polyester. This further supports that the polymer structure possessed  
28 unique amphiphilic nature to produce self-assembled micellar structure in the aqueous  
29 medium at micro-molar concentration range. The CAC of the drug or dye loaded samples  
30 could not be determined due to the overlap of fluorescence signals of the encapsulated dyes  
31 with pyrene. Thus, the DLS data of the nascent polymer with their dye and drug encapsulated  
32 polymer nanoparticles were compared to indirectly understand the stability. The DLS  
33 histograms of drug loaded polymer are provided in Figure S12 and support that the polymer  
34 nanoparticle size did not change before and after encapsulation of drugs or dyes. The above  
35 studies revealed that the custom-designed hydroxyl functionalized polymer nano-assemblies  
36  
37  
38  
39  
40  
41  
42  
43  
44  
45  
46  
47  
48  
49  
50  
51  
52  
53  
54  
55  
56  
57  
58  
59  
60

are very robust in encapsulating both water-soluble and water-insoluble drugs and fluorophore dyes without altering the size and shape of the nanoparticles.

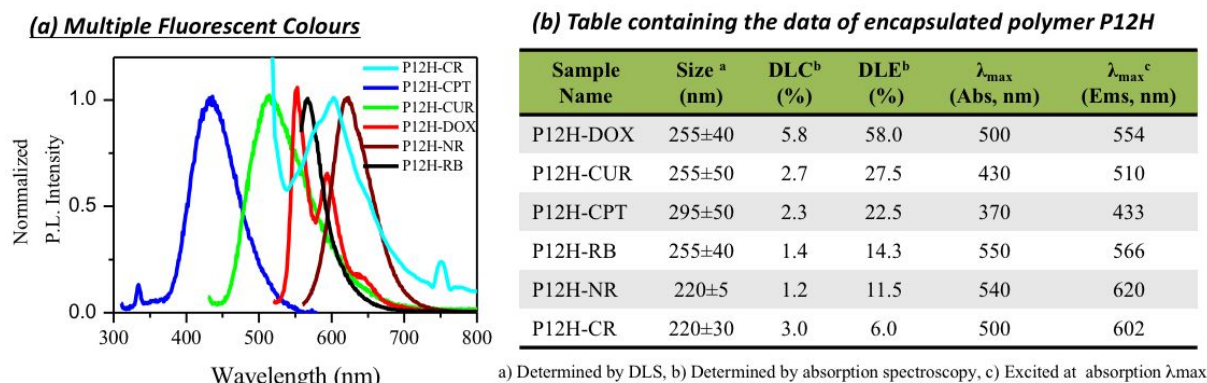


**Figure 5.** (a) Emission spectra of the drug and fluorophore encapsulated P12H nanoparticles ( $\lambda_{exc}$  = absorbance maxima). (b) The table containing the average size of the drug and fluorophore encapsulated P12H nanoparticles determined by DLS; drug loading content (DLC) determined by absorption spectroscopy, drug loading efficiency (DLE), their absorbance and emission maxima.

The drug molecules DOX, CPT, CUR and the dye molecules RB, NR, CR are highly luminescent molecules; thus, their absorbance and emission spectra were recorded for the aqueous nanoparticles. Absorbance spectra are shown in Figure S14 and their emission spectra are shown in Figure 5a. The DLS size of the nano-aggregates, their absorbance, and emission maxima values are shown in the table in Figure 5b. The encapsulated fluorophore dyes are predominantly red-color thus they exhibited absorbance maxima from 500-550 nm and emission maxima at 560-620 nm. On the other hand CPT, CUR and DOX loaded samples showed blue, green and red emission, respectively, with distant maxima at 433, 510 and 554 nm. Thus, the present approach provides significant color-tunability in terms of encapsulated drug or fluorophore dyes ranging from 300 to 650 nm in the entire visible light region in a single polymer nano-platform. The drug loading content (DLC) and drug loading efficiency (DLE) seems to be varying depending upon the loaded cargoes. DOX exhibited higher loading compared to all other molecules. Nevertheless, the number of drugs and fluorophore dyes are significant enough to study their cytotoxicity effect and bio-imaging in cell lines. Additionally, the present hydroxyl polymer system enabled the encapsulation of almost 6 different cargoes; thus, their cellular uptake studies would be valuable in the L-amino acid-based nano-carriers in the literature.

## Enzymatic-Biodegradation and Cytotoxicity Studies

The polymer backbone is designed with aliphatic ester chemical linkages which are well known to undergo biodegradable cleavage by lysosomal enzymes at the intracellular environment. Earlier attempts revealed that esterase enzymes and proteomic enzymes like trypsin and  $\alpha$ -chymotrypsin potentially degraded the aliphatic polyesters and aliphatic amide chemical linkages polymeric nanoassemblies.<sup>54</sup> To study the enzymatic biodegradation of the polymer backbone in P12H chains, the DOX loaded nanoparticle was subjected to *in vitro* drug release studies in the presence of various enzymes. *In vitro* drug release study was done by dialysis method and the drug release content was measured by absorption spectroscopy and the cumulative drug release was determined. In the absence of exposure to enzymes, the P12H-DOX nanoparticles experience extracellular like conditions; thus, the degree of the cleavage of the nanoparticles is expected to be minimum to nil. On the other hand, once the nanoparticles were taken across the cell membrane, they are readily exposed to the enzymes at the intracellular level for biodegradation to release the drugs as shown in Figure 6a. *In vitro* drug release data for the P12H-DOX nanoparticles in PBS at 37 °C (pH 7.4) is shown in Figure 6b. It was found that the doxorubicin encapsulated nanoparticles was stable in the nano-cavity under (in PBS) physiological conditions. To study the biodegradation of nano-scaffold by the lysosomal enzymes, the drug release kinetics was investigated by incubating the P12H-DOX in the presence of 10 U of three enzymes such as horse liver esterase, porcine liver esterase and  $\alpha$ -chymotrypsin from bovine pancreas in PBS at 37 °C (pH 7.4). These enzymes are known to cleave the aliphatic polyesters and aliphatic polyamide linkages which de-stabilize the loading capabilities of the polymer nanoparticles and released the cargoes.<sup>54</sup> Doxorubicin was found to be released nearly 40-50 % within 12 h exposure to these enzymes which was very significant compared to the release profiles in the absence of the enzymes (see Figure 6b). Among all three enzymes,  $\alpha$ -chymotrypsin was found to exhibit more biodegradation since it has capability to degrade both the polyester backbone and amide side-chain in P-12H structure. Surprisingly, the complete release of the doxorubicin from the nano-scaffold was not observed even after 36 h which is not clear at present. This may be partially due to the strong interaction of the hydroxyl units with DOX which restrict the enzymatic-biodegradation at large. Further structure-optimization of hydroxyl polyesters may be required in the long term to accomplish complete release of the drugs and validate this trend. The stability of the polymer nanoparticles were studied in different pH. The polymer nanoparticles were incubated at pH=4.0 (acetate buffer) <sup>68</sup> and pH=7.4 (PBS) and

their stability was studied using dynamic light scattering at 37 °C for 24 h (see Figure S15). It was found that the nanoparticles were stable in the acidic pH. This data further supports the observation in Figure 6b that the polymer nanoparticle was susceptible to biodegradation exclusively in the presence of enzymes. Nevertheless, the current design was able to release about 50 % of the drugs in a controlled manner upon exposure to lysosomal esterase enzymes which validated the intracellular drug-delivering capacities of the hydroxyl functionalized polyester nanoparticles.

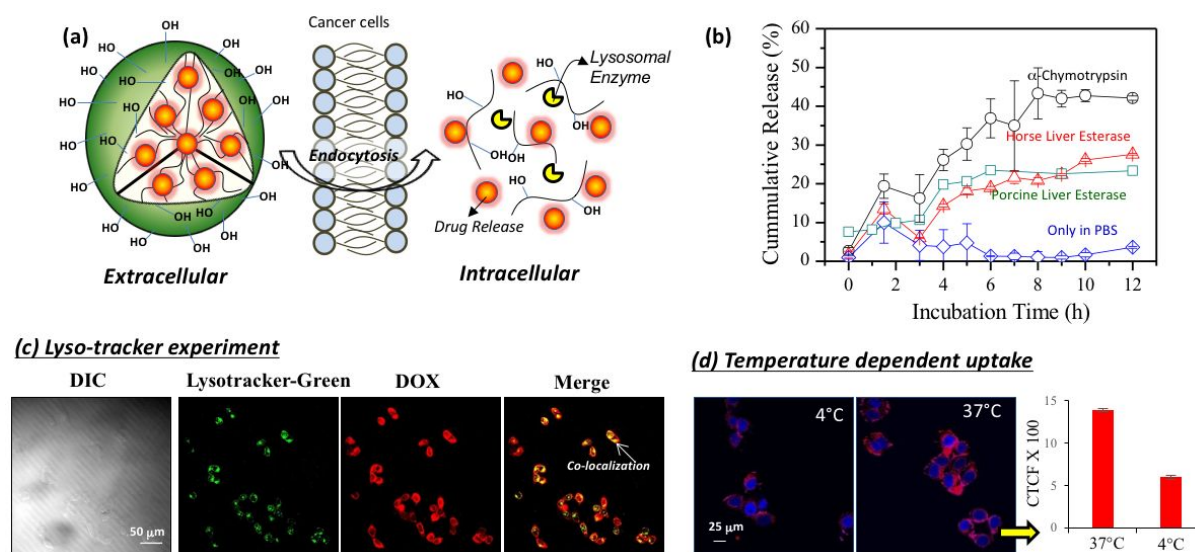


**Figure 6.** (a) Schematic representation of enzymatic-biodegradation of P12H-DOX nanoparticles at intracellular compartments. (b) Cumulative drug release profiles of P12H-DOX in the absence and in the presence of horse liver esterase enzyme,  $\alpha$ -chymotrypsin from bovine pancreas and porcine liver esterase at 37 °C and pH 7.4 in PBS. (c) Live-cell confocal microscopy imaging of P12H-DOX nanoparticles in the presence of lyso-tracker in HeLa cell line. The concentration of DOX is maintained as 20  $\mu$ M and incubated for 6h. (d) Confocal microscopy imaging of variable temperature dependent cellular uptake studies in HeLa fixed cells. The concentration of DOX is maintained as 20  $\mu$ M and incubated for 5h. (Scale bar in the cell images = 50  $\mu$ m and 25  $\mu$ m).

HeLa cells were chosen to carry out cellular uptake of P12H-DOX nanoparticles to corroborate the enzyme degradation at cellular levels. Since the lysosomes of cells are rich in hydrolytic enzymes, this experiment was carried out to establish the uptake of the nanoparticles via endocytosis. The P12H-DOX nanoparticles were incubated with HeLa cell in a live cell chamber for 6 h. The free dispersed nanoparticles in media that were not taken up by the cells, if any, were removed by aspirating the media. To rule out the possibility of the uptake of the nanoparticles by diffusion or another method, the lysosomes of the cells

1  
2  
3 were stained with highly selective LysoTracker Green DND dye. This staining was carried out  
4 immediately before the imaging of the live cells. The LysoTracker Green DND was excited at  
5 488 nm with laser power 2 ( keeping gain < 800) at 1.0 A.U. and was imaged in the green  
6 channel. The DOX moieties were excited at 561 nm laser and were imaged in the red  
7 channel. Smart set up was used to select the tracks for exciting the fluorophores to eliminate  
8 the cross-talk between the emission and excitation of the LysoTracker Green DND and DOX.  
9 The images thus obtained were processed in Image J software and were plotted and are  
10 shown figure 6c. The four panels show the differential interference contrast (DIC), lyso green  
11 channel, DOX channel and the merged channel (red and green channel merged). The DIC  
12 channel showed the cell position and morphology during the live cell experiment. The green  
13 channel showed the bright green color that emerged from the lysosomal compartments of the  
14 cellular regions. These regions are highly acidic in nature and are selectively stained by the  
15 Lyso-tracker Green DND. The third panel shows the DOX uptake in the HeLa cells in 6 h  
16 and it was observed that DOX emission was obtained from all over the cells with high-  
17 intensity regions in few places. On merging the green and the red channel it was observed  
18 that this high concentration of DOX was indeed present at the lysosomal regions, as the  
19 colocalization of lysosomes and DOX could only produce bright yellow emission (a mixture  
20 of red and green). Therefore, within 6h of incubation, the P12H-DOX successfully  
21 accumulated in the lysosomal compartments of the cell. The P12H nanoparticles were  
22 excellent carriers for DOX and selectively deliver the DOX in the HeLa cells as these would  
23 undergo lysosomal degradation, thereby releasing the drug into the cytoplasm.

24  
25  
26  
27  
28  
29  
30  
31  
32  
33  
34  
35  
36  
37  
38  
39  
40  
41 To further support the endocytosis assisted the uptake of the P12H nanoparticles in  
42 the cells a time dependent uptake experiment was carried out for fixed cell imaging. Since  
43 endocytosis is an energy-dependent process hence it is believed that any process occurring  
44 due to endocytosis should slow down at temperatures lower than the physiological  
45 temperatures.<sup>69-70</sup> Therefore, a temperature-dependent experiment was carried out wherein,  
46 P12H nanoparticles loaded with DOX, CUR, and CPT were incubated with cells at different  
47 temperatures. HeLa cells were seeded in two separate 6-well plates and grown for 24 h in an  
48 incubator with 5% CO<sub>2</sub> at 37 °C. After 24h the media from the cells were aspirated and 20.0  
49 μM of DOX, CUR and CPT in P12H-DOX, P12H-CUR, and P12H-CPT nanoparticles (in  
50 media) was added to the cells. One 6-well plate was incubated at 37 °C and the other plate  
51 was maintained at 4° C. The cells were fixed after 5h incubation. The cells in case of DOX  
52 chromophores were stained with DAPI prior to mounting on glass slides. Further, these cells  
53 were imaged. DAPI, CPT, and CUR were excited at 405 nm laser and were imaged in blue,  
54  
55  
56  
57  
58  
59  
60

1  
2  
3 blue and green channels respectively (see Figures S16 and Figure S17). The confocal images  
4 of the P12H-DOX at 4°C and 37°C have been shown in figure 6d. The merged image shows  
5 the DAPI stained blue nucleus and the red emission from the DOX distributed in cytoplasm  
6 of the cells. It was clearly evident that at lower temperatures such as 4°C the uptake of  
7 nanoparticles was low compared to the uptake at physiological temperature as red emission  
8 from the cells was observed more in case of 37°C. Further, the CTCF intensities of DOX  
9 were calculated and plotted in figure 6d. It was observed that uptake of DOX at 37°C was 3  
10 times higher compared to that at 4°C. This was evident because at lower temperature  
11 conditions the process of the endocytosis was slowed down and resulted in lesser uptake of  
12 the P12H nanoparticles. This was further extended to P12H-CPT and P12H-CUR  
13 nanoparticles and the images have been shown in Figures S16 and Figure S17. A similar  
14 trend was observed wherein lower emission was observed in the case of P12H nanoparticles  
15 incubated at 4 °C both in the blue (cyan) and green channel for CPT and CUR respectively.  
16 Whereas the cells showed higher uptake of the P12H-CPT and P12H-CUR at 37 °C, further  
17 illustrating the endocytosis dependent uptake of the nanoparticles in the cells. Since the size  
18 of free drugs is very less compared to nanoparticles (~ 5-10 nm), they are taken up by simple  
19 diffusion across the cell membrane. Therefore, it was anticipated that there should not be  
20 much difference in uptake of free drugs at either temperature. The uptake of the free drugs  
21 was found to be similar as seen in the Figure S16 Figure S17. Hence, compared to  
22 temperature-dependent uptake of free drugs, the P12H nanoparticles were taken up more in  
23 the cells and the same was corroborated by the live-cell experiments. It was found that the  
24 P12H nanoparticles accumulated in the lysosomes of the HeLa cells, which was essential for  
25 their biodegradation for the delivery of the loaded cargoes.  
26  
27  
28  
29  
30  
31  
32  
33  
34  
35  
36  
37  
38  
39  
40  
41  
42  
43  
44  
45  
46  
47  
48  
49  
50  
51  
52  
53  
54  
55  
56  
57  
58  
59  
60

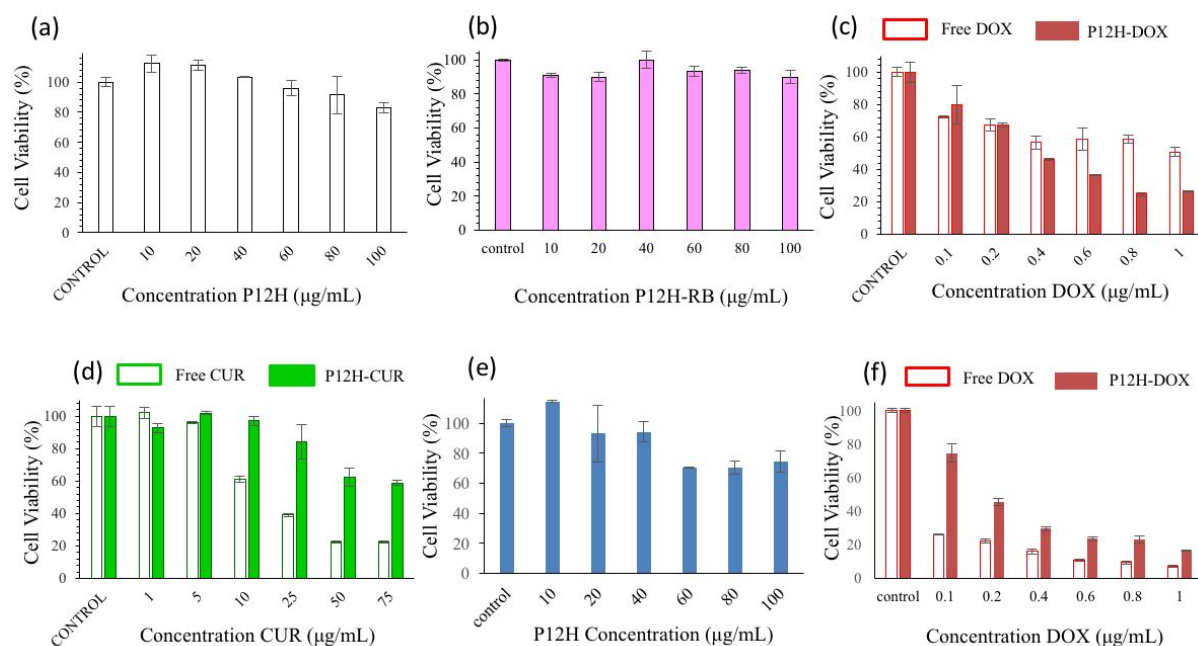


**Figure 7:** Cell viability of P12H nanoparticles (a), P12H-RB nanoparticles (b), free DOX and P12H-DOX nanoparticle (c), free CUR and P12H-CUR (d) in HeLa cells line at 37°C for 48 h. (e) Cell viability of P12H nanoparticles in WT-MEF cell line at 37°C for 48 h. (f) Cell viability of free DOX and P12H-DOX nanoparticle in WT-MEF cell lines at 37°C for 48 h.

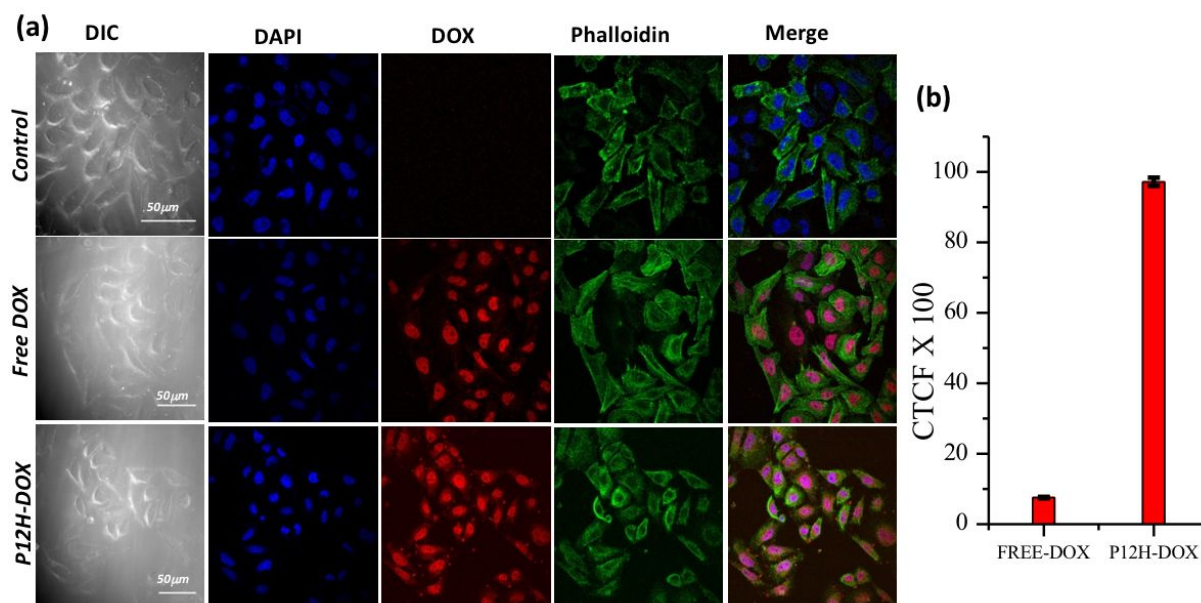
The biocompatibility of nascent polymer P-12H was investigated in cervical cancer cell lines (HeLa) and wild type mouse embryonic fibroblast (WT-MEF). As can be seen in Figure 7a, the nascent polymer nanoparticles were not cytotoxic to the HeLa cells even at a concentration up to 100  $\mu\text{g/mL}$  and were highly suitable as drug delivery carriers. These polymers exhibited the unique quality of being able to load and stabilize multiple dyes and drugs. The cytotoxicity profile in HeLa cells of the polymer nanoparticle loaded with Rose Bengal (P12H-RB) has been shown in Figure 7b, which exhibits that these dye loaded nanoparticles are highly biocompatible up to a concentration of 100  $\mu\text{g/mL}$ . The polymers also successfully encapsulated anticancer drugs like Doxorubicin and Curcumin and the anticancer efficacy of these drug loaded nanoparticles were studied in HeLa cell lines. For the free DOX and DOX-loaded nanoparticles (P12H-DOX), the concentration of the drug was varied from 0.1 to 1  $\mu\text{g/mL}$  and then the MTT assay was carried out after 48h of compound incubation. As can be seen in Figure 7c, the cell growth inhibition capability of the free drug saturated at a concentration of 0.4  $\mu\text{g/mL}$  and it was able to achieve 50 % cell killing at the concentration of 1.0  $\mu\text{g/mL}$ . On the other hand, the DOX-loaded nanoparticle was able to accomplish ~ 80 % cell growth inhibition and the  $\text{EC}_{50}$  value exhibited by these nanoparticles

1  
2  
3 was 0.4  $\mu\text{g/mL}$ , in accordance with the literature reports.<sup>70</sup> In the case of Curcumin, the  
4 concentration was ranged from 1 to 75  $\mu\text{g/mL}$  and the MTT assay is shown in figure 7d. The  
5 free Curcumin was able to achieve  $\sim 80\%$  cell killing with an  $\text{EC}_{50}$  value of 10  $\mu\text{g/mL}$   
6 whereas the polymer loaded curcumin (P12H-CUR) nanoparticles exhibited 50 % cell killing.  
7 Cytotoxicity data for P12H-CPT, P12H-NR, and P12H-CR are shown in the supporting  
8 information Figure S18. Based on the above studies, it may be summarized that the newly  
9 designed P12H polymer is very effective in inducing cell killing for the drug loaded nano-  
10 carriers (DOX, CPT and CUR) whereas their fluorophore (NR, CR, and RB) loaded  
11 nanoparticles are largely non-toxic to HeLa cell lines. In a similar way, P12H-DOX and  
12 P12H nanoparticles were also incubated with non-cancerous healthy cell lines WT-MEF  
13 (Wild- Type Mouse Embryonic Fibroblast cells) and the cell viability plots have been shown  
14 in Figures 7e and 7f. It was observed that significant cell killing ( $\sim 80\%$ ) was achieved by  
15 P12H-DOX loaded nanoparticles containing 1.0  $\mu\text{g/mL}$  DOX, whereas the higher amounts of  
16 the polymer ( $\sim 100$   $\mu\text{g/mL}$ ) showed extremely low toxicity towards the cells thereby  
17 demonstrating the effective therapeutic efficacy of the L-aspartic acid based newly designed  
18 P12H polyesters.  
19  
20  
21  
22  
23  
24  
25  
26  
27  
28  
29  
30  
31  
32  
33

### 34 Cellular Uptake Studies

35  
36  
37 The ability of the P12H-DOX nanoparticles as drug carrier was demonstrated by  
38 studying the cellular uptake of doxorubicin in HeLa and WT-MEF cell lines. The killing of  
39 cells occur via DNA intercalation mechanism of doxorubicin in the nucleus of the cell,  
40 therefore determination of the location of doxorubicin within the cell was crucial to analyze.  
41 HeLa cells were grown in a 6 well plate at a concentration of  $10^5$  cells in each well. The cells  
42 were further treated with doxorubicin, fixed and were subjected to confocal microscopy  
43 imaging. DAPI was used to stain the nucleus, and Alexa dye conjugated phalloidin green was  
44 used to illuminate cytoskeleton actin filaments network of the cells. This experiment was  
45 conducted to determine the location of the DOX molecules after the lysosomal accumulation  
46 of the nanoparticles in the cells (see figure 8). A control for cells without DOX was also  
47 maintained to rule out the possibility of signal interference from the other chromophores. The  
48 free doxorubicin and P12H-DOX nanoparticles were exposed to the HeLa cells keeping the  
49 concentration of the doxorubicin molecule same, to understand the efficacy of the nano-  
50 particle in drug delivery. The fixed cells were imaged using 405, 561 and 488 nm lasers for  
51  
52  
53  
54  
55  
56  
57  
58  
59  
60

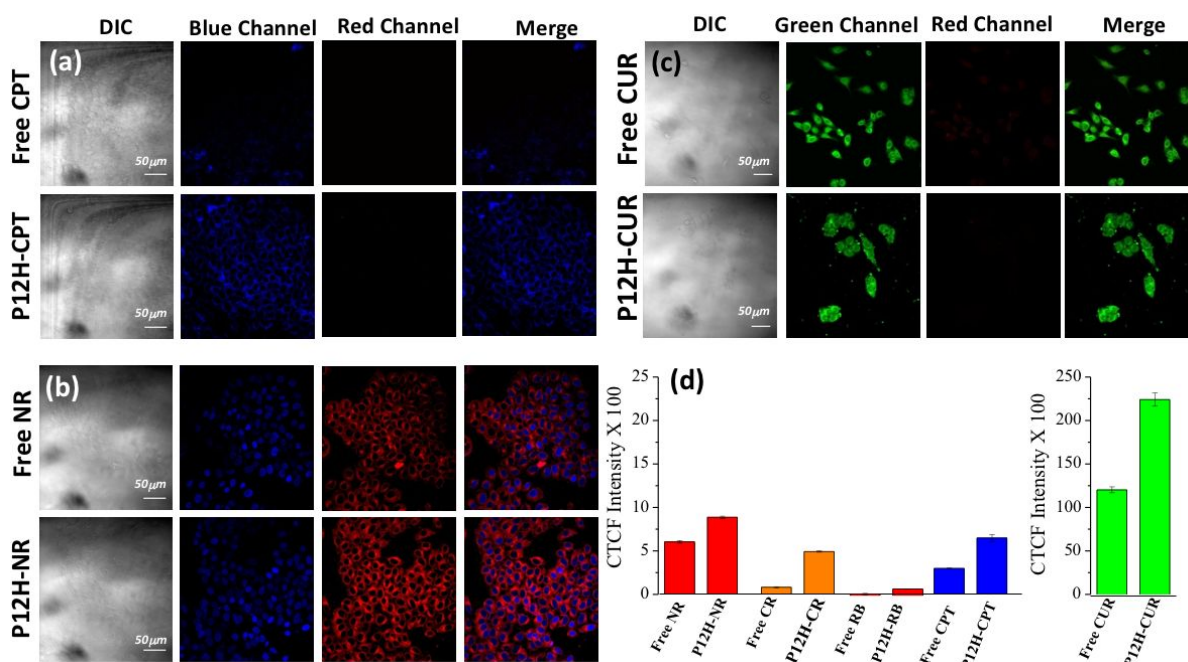
1  
2  
3 DAPI, DOX and Phalloidin respectively. The confocal images are shown in figure 8a. The  
4  
5 DIC images showed the fixed cells, and DAPI channel showed the nucleus in the cells, the  
6  
7 DOX channel showed the location of DOX molecules and the Phalloidin channel showed the  
8  
9 actin filaments of the cells. This was further merged in a fifth panel in figure 8a to show the  
10  
11 colocalization of the three fluorophores. The merged image shown in figure 8a showed clear  
12  
13 demarcation of the nucleus as well as doxorubicin uptake in the cells. Free DOX diffused in  
14  
15 the cells and was found to accumulate in the nucleus and was shown by the magenta color  
16  
17 because of the overlap of the DAPI and the DOX. The nanoparticles, however, were taken up  
18  
19 by the endocytosis and the DOX was delivered to the cytoplasm of the cells and it was found  
20  
21 to accumulate in the nucleus of the cells as shown in figure 8a. It was interesting to note that  
22  
23 the emission intensity of DOX from the nucleus was higher than the free DOX and it was a  
24  
25 qualitative-evidence towards higher uptake of the DOX in the cells. Therefore, the CTCF  
26  
27 calculations were carried out to quantify it and the plots have been shown in figure 8b. It was  
28  
29 observed that P12H-DOX carried ten folds higher DOX drug into the cells which is superior  
30  
31 compared to simple diffusion of free DOX across the cell membrane. Hence, the P12H-DOX  
32  
33 nanoparticles were capable of delivering DOX in to the cell, which would cause cell killing  
34  
35 which was reflected in the cytotoxicity data as shown in figure 7c. Doxorubicin is a small  
36  
37 molecular drug with size 50 Å; thus, it is known to efflux out from the cells through  
38  
39 membrane efflux pumps. On the other hand, the DOX loaded nanoparticles are significantly  
40  
41 larger in size; hence they localized in the cytosol for longer period which enhances the  
42  
43 probability of the DOX interaction with nucleus for increased cytotoxicity effect. Further, the  
44  
45 live cell cellular uptake studies clearly evident for the enhanced uptake of the DOX (see  
46  
47 Figure 6c) while delivered from the newly designed hydroxyl polymer P12H platform  
48  
49 compared to the free drug. Thus, both the nanoparticle design and the increased cellular  
50  
51 uptake enhanced the anticancer activity of P12H-DOX nanoparticle.  
52  
53  
54  
55  
56  
57  
58  
59  
60



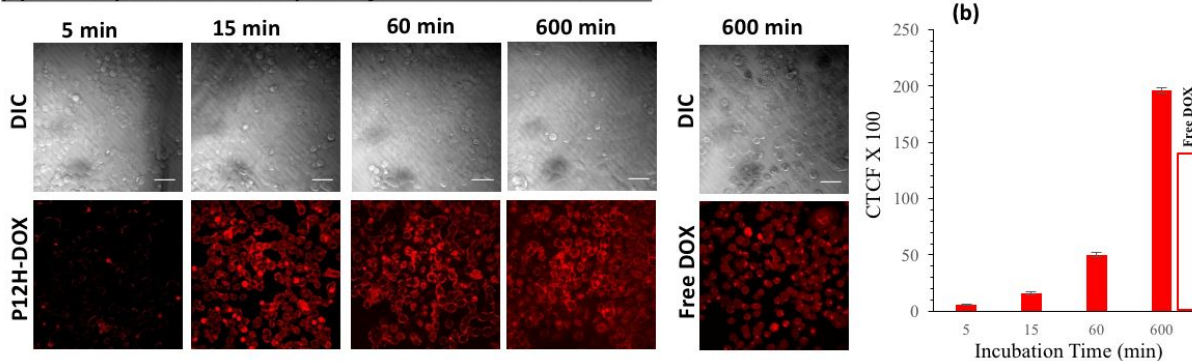
**Figure 8:** (a) The fixed cellular imaging of control cells (top most row), free DOX (second row) and P12H-DOX (third row) in HeLa cell lines. (b) CTCF intensity of free DOX and P12H-DOX uptake. The concentration of DOX was maintained as  $20\mu\text{M}$ . Cells were incubated for 6h at  $37\text{ }^{\circ}\text{C}$ . Scale bar represents  $50\mu\text{m}$  in cell images.

The multiple drug/dye loading capabilities of the hydroxyl functionalized P12H polymers were established by loading various drugs and dyes (hydrophobic and hydrophilic) and independent experiments were carried out to study their uptake at cellular levels. 10000 HeLa cells were seeded in each well of a 6 well plate and were grown for 24 h. The media from the cells were aspirated and they were exposed to P12H-CPT, P12H-CUR, P12H-NR, P12H-RB, P12H-CR nanoparticles. The concentration of the drugs and dyes were maintained as  $20.0\text{ }\mu\text{M}$  (Only RB and NR was taken as  $5.0\text{ }\mu\text{M}$ ), and the cells were incubated for 5 h in a  $\text{CO}_2$  incubator at  $37\text{ }^{\circ}\text{C}$ . The corresponding free drugs and dyes were also incubated with the cells to draw comparisons in the cellular uptake. The cells were imaged using a confocal microscope using various lasers like 405 nm for CPT and CUR which were imaged in blue and green channels respectively. CR, NR, and RB were excited using lasers 488, 514 and 561 nm lasers and were imaged under the red channel. The versatile nature of loading drugs and dyes in various regions of visible spectra were demonstrated by P12H nanoparticles and their corresponding imaging has been shown in figure 9. Figure 9a shows comparative uptake of P12H-CPT and free CPT in HeLa cells and it was observed more cells endocytosed the CPT compared to diffusion in case of free CPT. The channel showed the higher distribution of the

CPT within the cells through P12H-CPT nanoparticles. No emission in the red channel ruled out auto-fluorescence from the cells. The figure 9b shows the comparative uptake of NR in the free state and in P12H-NR form. The nucleus of the cells was stained with DAPI and it was observed that the NR showed higher emission as it was delivered to cytoplasm of cells in higher amount compared to free counterpart. A similar observation was seen in free CUR and P12H-CUR wherein high green emission was observed in the case of CUR delivered by the nanoparticles (see figure 9c). The same trend was demonstrated in the case of RB and CR free and nanoparticle delivery and the images are shown in Figures S19 and S20. The cellular uptake trend in free cargo and polymer loaded cargoes was further quantified by calculating the CTCF intensities of the drugs and dyes at the cellular level. Figure 9d shows the P12H nanoparticles could transport the loaded drugs and dyes almost two-fold higher than their free counterparts. The hydroxyl functionalized polyester P12H nanoparticles proved to be a highly promising carrier for loading and delivering a wide range of anticancer drugs and fluorophore dye molecules to the intracellular compartments of the cancer cells.



**Figure 9.** (a) The fixed cell imaging of (a) free CPT and P12H-CPT, (b) free NR and P12H-NR, (c) free CUR and P12H-CUR in HeLa cell line. (d) CTCF intensity of free NR, CR, RB, CPT, CUR and P12H-NR, P12H-CR, P12H-RB, P12H-CPT, and P12H-CUR. The concentration of CPT and CUR were maintained as 20 μM. The concentration of NR was maintained as 5 μM. Cells were incubated for 6h at 37 °C. Scale bar represents 50 μm in cell images.

**(a) Time-dependent cellular uptake of P12H-DOX in HeLa Cell line**

**Figure 10.** (a) Time-dependent live cell imaging of P12H-DOX at time 5, 15, 60 and 600 min and free DOX at 600 min. (b) CTCF intensity of P12H-DOX at time 5, 15, 60 and 600 min and free DOX at 600 min. The concentration of DOX was maintained as  $20\mu\text{M}$ . Scale bar represents  $50\mu\text{m}$  in cell images.

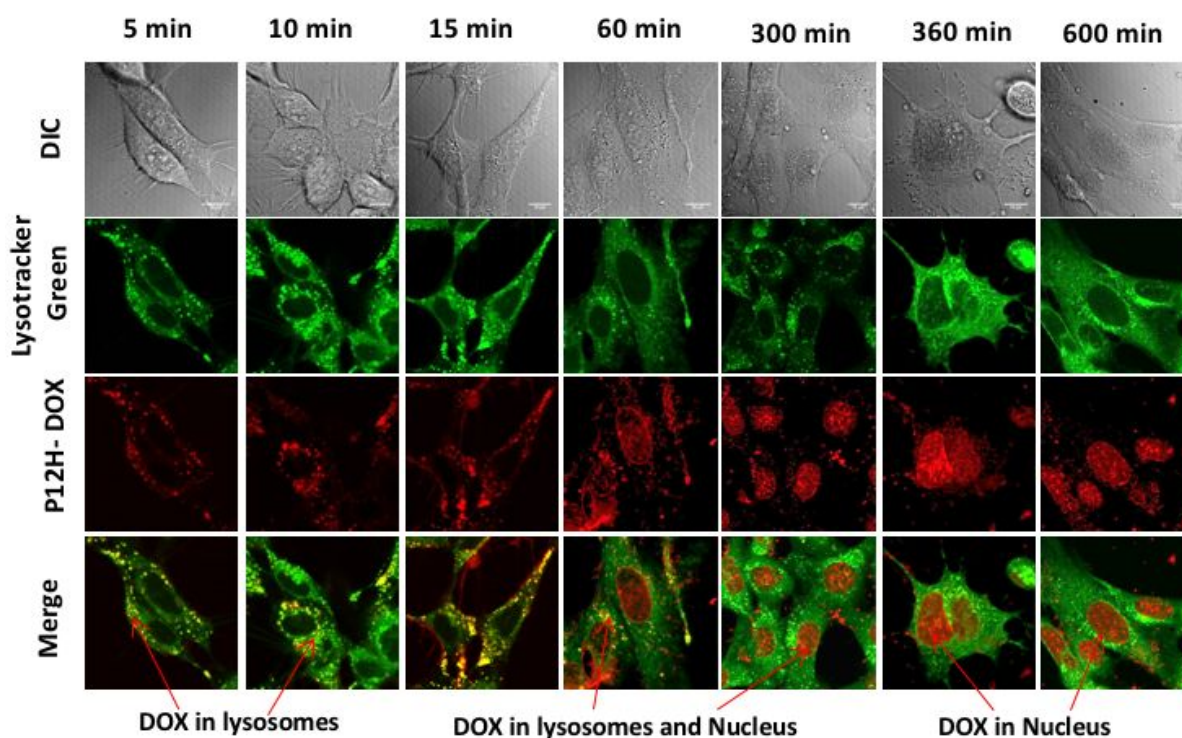


**Figure 11.** (a) Time-dependent live cell imaging of P12H-DOX at time 5, 10, 15, 60, 300, 360 and 600 min in Wild Type-Mouse Embryonic Fibroblast, WT-MEF). The concentration of DOX was maintained as  $20\mu\text{M}$ . Scale bar represents  $10\mu\text{m}$  in cell images.

1  
2  
3 Further to quantify the kinetics of uptake of P12H nanoparticles against time, the  
4 P12H-DOX nanoparticles were chosen and their real-time uptake was monitored using live-  
5 cell uptake experiments. P12H-DOX nanoparticles (containing 20.0  $\mu\text{M}$  DOX) were exposed  
6 to HeLa cell line at time points ranging from 5, 15, 60 and 600 min. Free DOX (20.0  $\mu\text{M}$ )  
7 was also exposed to the live cells for 600 min as a control to compare maximum uptake in the  
8 cells. LysoTracker Green DND-26 was used for selective staining of the lysosomal  
9 compartments of the cells. The lysosomes were excited using laser 488nm and DOX was  
10 excited using 561 nm laser and imaged under green and red channel respectively. The images  
11 processed in Image J software were shown in figure 10a. The first panel shows the DIC and  
12 residual red emission from the cells in 5 minutes incubation. The intensity of red emission  
13 increased in 15 minutes incubation time as observed in the second panel. The intensity of  
14 DOX emission increased rapidly upon increasing the incubation time of the nanoparticles in  
15 the live cells until 600 min. Free DOX uptake was carried out for 10 h and the images are  
16 shown in figure 10a last panel. The CTCF (corrected total cell fluorescence) plots were  
17 generated using Image J software for 8-bit images using set of 3 independent cells, and the  
18 time-dependent plot for cellular uptake was generated and the plots are shown in figure 10 b.  
19 The intensity of the DOX red emission increased 200 folds higher from 5 minutes to 10 h  
20 which was indicative of continuous uptake of P12H-DOX nanoparticles, essential for cell  
21 killing applications. The free DOX counterpart showed less intensity compared to P12H-  
22 DOX showing the efficacy of the nanoparticles as drug carriers. Further the cellular uptake of  
23 the P12H-DOX nanoparticle was also investigated in live cell imaging experiment in non-  
24 cancerous WT-MEF cell lines as shown in Figure 11. The cells were incubated at various  
25 times and were stained with lysotracker green DND -26 dye to study the endosome assisted  
26 uptake of the nanoparticles. The confocal microscopy images for the initial uptake of the  
27 P12H-DOX nanoparticles showed (up to 15 minutes) that the nanoparticle co-localized with  
28 the lysosomes and they were predominantly present in the cytosol of the cells (see Figure 11)  
29 This was observed as yellow merge emission of red DOX and green lysosomes as shown in  
30 the figure 11. For other images see figure S21. No emission was observed from the nucleus.  
31 At 1h incubation, the merged images showed green emission from lysosomes and red  
32 emission from nucleus of the cells. This indicated that the nanoparticles co-localized in the  
33 lysotracker due to the initial endosomal uptake, may have undergone degradation by the  
34 enzymes present in the lysosomes, resulting in release of the DOX which eventually  
35 accumulated in the nucleus. As result the nucleus became slightly red in colour due to the  
36 presence of DOX as shown in the merged images. With increase in the incubation time (from  
37  
38  
39  
40  
41  
42  
43  
44  
45  
46  
47  
48  
49  
50  
51  
52  
53  
54  
55  
56  
57  
58  
59  
60

1  
2  
3 5 to 10 h), more DOX was accumulated in the nucleus and the emission of DOX depleted  
4 significantly in the cytosol. This observation clearly supports both the cellular uptake of the  
5 P12H-DOX nanoparticles and their biodegradation by the lysosomal enzymes as the  
6 mechanism proposed in Figures 1. Further, the uptake study was also performed for free  
7 DOX under the similar conditions in WT-MEF cells and the details are shown in Figure S22.  
8 It is very interesting to find that the cellular uptake of the DOX increases with the incubation  
9 time and attained maxima at 10 h. The 10 h incubation data for free DOX and P12H-DOX  
10 clearly showed that the DOX was delivered more from the nanoparticle platform. The cellular  
11 uptake studies of P12H polymer nanoparticles in cancer cell line (HeLa) and normal cell line  
12 (WT-MEF) showed similar trend for the DOX uptake in 2D cell line experiments. The  
13 difference in accumulation or uptake of drugs will be more pronounced through enhanced  
14 permeability retention effect in the *in vivo* model which will be done in future studies.  
15 Nevertheless, the present investigation has clearly demonstrated that the hydroxyl  
16 functionalized polyester nano-carriers are an excellent platform to administrate a wide range  
17 of anticancer drugs and fluorophore dye molecules to the intracellular compartments of the  
18 cancer cells. The concept is successfully proven for half a dozen cargoes, both water soluble  
19 and water insoluble drugs and dyes in cervical cancer cell lines. This polymer design is not  
20 restricted to particular cancer cell lines or drug molecules; in general and this approach can  
21 be explored to a wide variety of other systems as well. Further, the hydroxyl functional  
22 groups could also be explored for anchoring targeted molecules, drugs or be employed as the  
23 functional handle for cross-linking chemistry to produce hydrogels and organogels, etc. At  
24 present, the research work is being expanded to increase the scope of the hydroxyl  
25 functionalized biodegradable polyester platform in the biomedical field.  
26  
27  
28  
29  
30  
31  
32  
33  
34  
35  
36  
37  
38  
39  
40  
41  
42

## 43 **Conclusion**

44  
45  
46 In summary, new classes of L-amino acid based biodegradable hydroxyl functional  
47 polyesters were designed and developed by solvent-free melt polycondensation approach  
48 from L-aspartic acid resources. A new multi-functional monomer from L-aspartic acid  
49 having acetal protecting group and di-carboxylic esters were tailor-made. The methyl esters  
50 of the aspartic acid monomer underwent melt-transesterification with commercial diols to  
51 produce high molecular weight acetal-functionalized polyesters under melt-transesterification  
52 process. Acid-assisted deprotection of these polymers yielded hydroxyl functionalized  
53 polyesters having bis-hydroxyl groups in each repeating unit of the polymer. The acetal and  
54 hydroxyl functionalized polymers were well characterized using proton and carbon NMRs  
55  
56  
57  
58  
59  
60

1  
2  
3 which showed building up of high molecular weight polymers. The GPC analyses further  
4 showed the monomodal distribution and the formation of high molecular weight polyesters.  
5 The thermal properties of the polyester using TGA analyses showed that these polymers were  
6 stable up to 300 °C and DSC analysis revealed that they were amorphous in nature. The  
7 hydrophilic hydroxyl groups along with the hydrophobic aliphatic backbone made these  
8 polymers amphiphilic in nature and enabled these to self-assemble into spherical  
9 nanoparticles in water. Anticancer drugs (DOX and CPT) and anti inflammatory drug CUR  
10 were successfully loaded in these nano-carriers. Both water-soluble (RB) and water-insoluble  
11 (NR and CR) fluorophore dyes were also encapsulated. *In vitro* drug release profiles and  
12 lyso-tracker assisted confocal microscopy images are evident for the enzymatic-  
13 biodegradation of the polyester nano-carriers and their ability to deliver the drugs at the  
14 intracellular level. Live cell cellular uptake studies confirmed the internalization of drug  
15 molecules at the intracellular level and supported the ability of these new hydroxyl polyester  
16 platform to exhibit excellent cell killing in HeLa cancer cell lines. The present investigation  
17 explored the un-known territory in the L-amino acid bioresources and opened up a new  
18 avenue for hydroxyl functionalized polyesters and their drug delivering capabilities in cancer  
19 cells which are completely new in the literature and is expected to have long-term impact in  
20 biomaterial research.  
21  
22  
23  
24  
25  
26  
27  
28  
29  
30  
31  
32  
33  
34  
35  
36  
37  
38  
39  
40  
41  
42  
43  
44  
45  
46  
47  
48  
49  
50  
51  
52  
53  
54  
55  
56  
57  
58  
59  
60

## ASSOCIATED CONTENT

**Supporting Information:** Polymer synthetic data,  $^1\text{H}$ ,  $^{13}\text{C}$  NMR, DSC and TGA thermograms of monomer polymers, polymer kinetics data, DLS data, FE-SEM images, absorption spectra and the cellular uptake data of RB and CR loaded samples have been provided in the supporting information. The Supporting Information is available free of charge on the [ACS Publications website](#)

## AUTHOR INFORMATION

### Author Contributions

The manuscript was written through contributions of all authors. All authors have given approval to the final version of the manuscript. The authors declare no competing financial interest.

**Corresponding Author:** E-mail: [jayakannan@iiserpune.ac.in](mailto:jayakannan@iiserpune.ac.in).

## ACKNOWLEDGMENT

The authors thank Science and Engineering Research Board (SERB), New Delhi, Govt. of India for funding the project. Microscopy facility at IISER Pune is acknowledged.

## References

1. Iwata, T. Biodegradable and Bio-Based Polymers: Future Prospects of Eco-Friendly Plastics. *Angew. Chem. Int. Ed.* **2015**, *54*, 3210-3215.
2. Yao, K.; Tang, C. Controlled Polymerization of Next Generation Renewable Monomers and Beyond. *Macromolecules* **2013**, *46*, 1689-1712.
3. Partlow, P. B.; Applegate, M. B.; Omenetto, F. G.; Kaplan, D. L. Dityrosine Cross-Linking in Designing Biomaterials. *ACS. Biomater. Sci. Eng.* **2016**, *2*, 2108-2121.
4. Anitha, A.; Sowmya, S.; Kumar, P. T. S.; Deepthi, S.; Chennazhi, K. P.; Ehrlich, H.; Tsurkan, M.; Jayakumar, R. Chitin and Chitosan in Selected Biomedical Applications. *Progress in Polymer Science* **2014**, *39*, 1644-1667.
5. Khan, W.; Muthupandian, F.; Farah, S.; Kumar, N. Domb, A. J. Biodegradable Polymers Derived From Amino Acids. *Macromol. Biosci.* **2012**, *11*, 1625-1636.
6. Lalatsa, A.; Schatzlein, A. G.; Mazza, M.; Le, T. B. H.; Uchegbu, I. F. Amphiphilic poly(l-amino acids) - New materials for drug delivery. *J. Control. Release* **2012**, *161*, 523-536.
7. Sun, H.; Meng, F.; Dias, A. A.; Hendriks, M.; Feijen, J.; Zhong, Z.  $\alpha$ -Amino Acid Containing Degradable Polymers as Functional Biomaterials: Rational Design, Synthetic Pathway, and Biomedical Applications. *Biomacromolecules* **2011**, *12*, 1937-1955.
8. Bauri, K.; Nandi, M.; De, P. Amino Acid-Derived Stimuli-Responsive Polymers and Their Applications. *Polym. Chem.* **2018**, *9*, 1257-1287.
9. Deming, T. J. Methodologies for Preparation of Synthetic Block Copolypeptides: Materials with Future Promise in Drug Delivery. *Adv. Drug Deliv. Rev.* **2002**, *54*, 1145-1155.
10. Kramer, J. R.; Deming, T. J. Preparation of Multifunctional and Multireactive Polypeptides via Methionine Alkylation. *Biomacromolecules* **2012**, *13*, 1719-1723.
11. Deming, T. J. Polypeptide Materials: New Synthetic Methods and Applications. *Adv. Mater.* **1997**, *9*, 299-311.
12. Shen, Y.; Fu, X.; Fu, W.; Li, Z. Biodegradable Stimuli-Responsive Polypeptide Materials Prepared by Ring Opening Polymerization. *Chem. Soc. Rev.* **2015**, *44*, 612-622.
13. Cai, C.; Wang, L.; Lin, J. Self-assembly of Polypeptide Based Copolymers into Diverse Aggregates. *Chem. Commun.* **2011**, *47*, 11189-11203.
14. Yin, Q.; Yin, L.; Wang, H.; Cheng, J. Synthesis and Biomedical Applications of Functional Poly( $\alpha$ -hydroxy acids) via Ring-Opening Polymerization of O-Carboxyanhydrides. *Acc. Chem. Res.* **2015**, *48*, 1777-1787.
15. Basu, A.; Kunduru, K. R.; Katzhendler, J.; Domb, A. J. Poly( $\alpha$ -hydroxy acid)s and Poly( $\alpha$ -hydroxy Acid-co- $\alpha$ -amino acid)s Derived from Amino Acid. *Adv. Drug Deliv. Rev.* **2016**, *107*, 82-96.
16. Osada, K.; Kataoka, K. Drug and Gene Delivery Based Supramolecular Assembly of PEG-Polypeptide Hybrid Block Copolymer. *Adv. Polym. Sci.* **2006**, *202*, 113-153.

17. Carlsen, A.; Lecommandoux, S. Self-Assembly of Polypeptide Based Block Copolymer Amphiphiles. *Current Opinion in Colloid & Interface Science* **2009**, *14*, 329-339.
18. Deming, T. J. Synthetic Polypeptides for Biomedical Applications. *Prog. Poly. Sci.* **2007**, *32*, 858-875.
19. Cui, H.; Liu, Y.; Deng, M.; Pang, X.; Zhang, P.; Wang, X.; Chen, X.; Wei, Y. Synthesis of Biodegradable and Electroactive Tetraaniline Grafted Poly(ester amide) Copolymers for Bone Tissue Engineering. *Biomacromolecules* **2012**, *13*, 2881-2889.
20. Asin, L.; Armelin, E.; Montane, J.; Rodriguez-Galan, A.; Puiggali, J. Sequential Poly(ester amide)s Based on Glycine, Diols, and Dicarboxylic Acids: Thermal Polyesterification Versus Interfacial Polyamidation. Characterization of Polymers Containing Stiff Units. *J. Polym. Sci., Part A: Polym. Chem.* **2001**, *39*, 4283-4293.
21. Mejia, J. S.; Gillies, E. R. Triggered Degradation of Poly(ester amide)s via Cyclization of Pendent Functional Groups of Amino Acid Monomers. *Poly. Chem.* **2013**, *4*, 1969-1982.
22. Wu, J.; Chu, C.C. Water Insoluble Cationic Poly(ester amide)s: Synthesis, Characterization and Applications. *J. Mater. Chem. B.* **2013**, *1*, 353-360.
23. Sun, H.; Cheng, R.; Deng, C.; Meng, F.; Dias, A. A.; Hendriks, M.; Feijen, J.; Zhong, Z. Enzymatically and Reductively Degradable  $\alpha$ -Amino Acid-Based Poly(ester amide)s: Synthesis, Cell Compatibility, and Intra Cellular Drug Delivery. *Biomacromolecules*, **2015**, *16*, 597-605.
24. Sommerfeld, S. D.; Zhang, Z.; Costache, M. C.; Vega, S. L.; Kohn, J. Enzymatic Surface Erosion of High Tensile Strength Polycarbonates Based on Natural Phenols. *Biomacromolecules* **2014**, *15*, 830-836.
25. Kim, J.; Magno, M. H. R.; Alvarez, P.; Darr, A.; Kohn, J.; Hollinger, J. O. Osteogenic Differentiation of Pre-Osteoblasts on Biomimetic Tyrosine-Derived Polycarbonate Scaffolds. *Biomacromolecules* **2011**, *12*, 3520-3527.
26. Yu, C.; Kohn, J. Tyrosine-PEG-derived poly(ether carbonate)s as New Biomaterials Part I: Synthesis and Evaluation. *Biomaterials*, **1999**, *20*, 253-264.
27. Tangpasuthadol, V.; Shefer, A.; Hooper, K. A.; Kohn, J. Thermal Properties and Physical Ageing Behaviour of Tyrosine-derived Polycarbonates. *Biomaterials*, **1996**, *17*, 463-468.
28. Bourke, S. L.; Kohn, J. Polymers derived from the amino acid L-tyrosine: polycarbonates, Polyarylates and Copolymers with Poly(ethylene glycol). *Adv. Drug Deliv. Rev.* **2003**, *55*, 447-466.
29. Sheihet, L.; Piotrowska, K.; Dubin, R. A.; Kohn, J.; Devore, D. Effect of Tyrosine-Derived Triblock Copolymer Compositions on Nanosphere Self-Assembly and Drug Delivery. *Biomacromolecules* **2007**, *8*, 998-1003.
30. He, M.; Ro, L.; Liu, J.; Chu, C. C. Folate Decorated Arginine Based Poly(ester urea urethane) Nanoparticles as Carriers for Gambogic Acid and Effect on Cancer Cells. *J Biomed Mater Res. Part A.* **2017**, *105*, 475-490.
31. He, M.; Potuck, A.; Khon, J. C.; Fung, K.; King, C. A. R.; Chu, C. C. Self-Assembled Cationic Biodegradable Nanoparticles from pH-Responsive Amino-Acid-

- Based Poly(Ester Urea Urethane)s and Their Application As a Drug Delivery Vehicle. *Biomacromolecules* **2016**, *17*, 523-537.
32. Wu, J.; Wu, D.; Mutschler, M. A.; Chu, C. C. Cationic Hybrid Hydrogels from Amino Acid Based Poly(ester amide): Fabrication, Characterization, and Biological Properties. *Adv. Funct. Mater.* **2012**, *22*, 3815-2823.
33. Liu, J.; Wang, P.; Chu, C. C.; Xi, T. Arginine- Leucine Based Poly(ester urea-urethane) Coating for Zn-Y-Nd Alloy in Cardiovascular Stent Applications. *Colloids Surf. B* **2017**, *159*, 78-88.
34. Childers, E. P.; Peterson, G. I.; Ellenberger, A. B.; Domino, K.; Seifert, G. V.; Becker, M. L. Adhesion of Blood Plasma Proteins and Platelet-rich Plasma on L-Valine-Based Poly(ester urea). *Biomacromolecules* **2016**, *17*, 3396-3403.
35. Bhagat, V.; O'Brien, E.; Zhou, J.; Becker, M. L. Caddisfly Inspired Phosphorylated Poly(ester urea)-Based Degradable Bone Adhesives. *Biomacromolecules* **2016**, *17*, 3016-024.
36. Peterson, G. I.; Dobrynin, A. V.; Becker, M. L.  $\alpha$ -Amino Acid-Based Poly(ester urea)s as Multishape Memory Polymers for Biomedical Applications. *ACS Macro Lett.* **2016**, *5*, 1176-1179.
37. Dreger, N. Z.; Wndel, M. B.; Robinson, L. L.; Luong, D.; Sondergaard, C. S.; Hiles, M.; Premanandan, C.; Becker, M. L. Preclinical in Vitro and in Vivo Assessment of Linear and Branched L-Valine-Based Poly(ester urea)s for Soft Tissue Applications. *ACS Biomater. Sci. Eng.* **2018**, *4*, 1346-1356.
38. Chen, K.; Dreger, N. Z.; Pang, F.; Vogt, B. D.; Becker, M. L. Nonlinear Mechano-Optical Behavior and Strain-Induced Structural Changes of L-Valine-Based Poly(ester urea)s. *Macromolecules* **2018**, *51*, 8114-8126.
39. Peterson, G. I.; Childers, E. P.; Andery, H. L.; Dobrynin, A. V.; Becker, M. L. Tunable Shape Memory Polymers from  $\alpha$ -Amino Acid-Based Poly(ester urea)s. *Macromolecules* **2017**, *50*, 4300-4308.
40. Wu, J.; Zhao, L.; Xu, X.; Bertrand, N.; Choi, W.; Yameen, B.; Shi, J.; Shah, V.; Mulvale, M.; MacLean, J. L.; Farokhzad, O. C. Hydrophobic Cysteine Poly(disulfide)-based Redox-Hypersensitive Nanoparticle Platform for Cancer Theranostics. *Angew. Chem. Int. Ed.* **2015**, *54*, 9218-9223.
41. Lu, W.; Wang, X.; Cheng, R.; Deng, C.; Meng, F.; Zhong, Z. Biocompatible and Bio reducible Micelles Fabricated from Novel  $\alpha$ -Amino Acid-based Poly(disulfide urethane)s: Design, Synthesis and Triggered Doxorubicin Release. *Polym. Chem.* **2015**, *6*, 6001-6010.
42. Ling, X.; Chen, X.; Riddell, I. A.; Tao, W.; Wang, J.; Hollett, G.; Lippard, S. J.; Farokhzad, O. C.; Shi, J.; Wu, J. Glutathione-Scavenging Poly(disulfide amide) Nanoparticles for the Effective Delivery of Pt(IV) Prodrugs and Reversal of Cisplatin Resistance. *Nano Lett.* **2018**, *18*, 4618-4625.
43. Huang, F.; Cheng, R.; Meng, F.; Deng, C.; Zhong, Z. Micelles Based on Acid Degradable Poly(acetal urethane): Preparation, pH-Sensitivity, and Triggered Intracellular Drug Release. *Biomacromolecules* **2015**, *16*, 2228-2236.

- 1  
2  
3  
4  
5  
6  
7  
8  
9  
10  
11  
12  
13  
14  
15  
16  
17  
18  
19  
20  
21  
22  
23  
24  
25  
26  
27  
28  
29  
30  
31  
32  
33  
34  
35  
36  
37  
38  
39  
40  
41  
42  
43  
44  
45  
46  
47  
48  
49  
50  
51  
52  
53  
54  
55  
56  
57  
58  
59  
60
44. Anantharaj, S.; Jayakannan, M. Polymers from Amino Acids: Development of Dual Ester-urethane Melt Condensation Approach and Mechanistic Aspects. *Biomacromolecules* **2012**, *13*, 2446-2455.
  45. Anantharaj, S.; Jayakannan, M. Catalyst and Temperature Driven Melt Polycondensation Reaction for Helical Poly(ester-urethane)s Based on Natural L-Amino acids. *J. Polym. Sci., Part A: Polym. Chem.* **2016**, *54*, 1065-1077.
  46. Aluri, R.; Jayakannan, M. Development of L-Tyrosine-Based Enzyme-Responsive Amphiphilic Poly(ester-urethane) Nanocarriers for Multiple Drug Delivery to Cancer Cells. *Biomacromolecules* **2017**, *18*, 189-200.
  47. Aluri, R.; Jayakannan, M. One-pot Two Polymers: ABB' Melt Polycondensation for Linear Polyesters and Hyperbranched Poly(ester-urethane)s Based on Natural L-Amino acids. *Polym. Chem.* **2015**, *6*, 4641-4649.
  48. Anantharaj, S.; Jayakannan, M. Amyloid-like Hierarchical Helical Fibrils and Conformational Reversibility in Functional Polyesters Based on L-Amino acids. *Biomacromolecules* **2015**, *16*, 1009-1020.
  49. Anantharaj, S.; Jayakannan, M. Melt Polycondensation Approach for Reduction Degradable Helical Polyester Based on L-Cystine. *J. Polym. Sci., Part A: Polym. Chem.* **2016**, *54*, 2864-2875.
  50. Saxena, S.; Jayakannan, M. Enzyme and pH Dual Responsive L-Amino Acid Based Biodegradable Polymer Nanocarrier for Multidrug Delivery to Cancer Cells. *J. Polym. Sci., Part A: Polym. Chem.* **2016**, *54*, 3279-3293.
  51. Aluri, R.; Saxena, S.; Joshi, D. C.; Jayakannan, M. Multistimuli-responsive Amphiphilic Poly(ester-urethane) Nanoassemblies Based on L-Tyrosine for Intracellular Drug Delivery to Cancer Cells. *Biomacromolecules* **2018**, *19*, 2166-2181.
  52. Joshi, D. C.; Saxena, S.; Jayakannan, M. Development of L-Tyrosine Based Biodegradable Polyurethanes and Their Dual-Responsive Amphiphilic Nanocarriers for Drug Delivery to Cancer Cells. *ACS Appl. Polym. Mater.* **2019**, *1*, 1866-1880.
  53. Ghaffar, A.; Draaisma, G. J. J.; Mihov, G.; Dias, A. A.; Schoenmakers, P. J.; van der Wal, S. Monitoring the in Vitro Enzyme-Mediated Degradation of Degradable Poly(ester amide) for Controlled Drug Delivery by LC-ToF-MS. *Biomacromolecules* **2011**, *12*, 3243-3251.
  54. Saxena, S.; Jayakannan, M.  $\pi$ -Conjugate Fluorophore-Tagged and Enzyme-Responsive L-Amino Acid Polymer Nanocarrier and Their Color-Tunable Intracellular FRET Probe in Cancer Cells. *Biomacromolecules* **2017**, *18*, 2594-2609.
  55. Saxena, S.; Pradeep, A.; Jayakannan, M. Enzyme-Responsive Theranostic FRET Probe Based on L-Aspartic Amphiphilic Polyester Nanoassemblies for Intracellular Bioimaging in Cancer Cells. *ACS Appl. Bio Mater.* **2019** ASAP 10.1021/acsbm.9b00450.
  56. Yu, J.; Xu, Y.; Li, S.; Seifert, G. V.; Becker, M. L. Three-Dimensional Printing of Nano Hydroxyapatite/Poly(ester urea) Composite Scaffolds with Enhanced Bioactivity. *Biomacromolecules* **2017**, *18*, 4171-4183.

- 1  
2  
3  
4  
5  
6  
7  
8  
9  
10  
11  
12  
13  
14  
15  
16  
17  
18  
19  
20  
21  
22  
23  
24  
25  
26  
27  
28  
29  
30  
31  
32  
33  
34  
35  
36  
37  
38  
39  
40  
41  
42  
43  
44  
45  
46  
47  
48  
49  
50  
51  
52  
53  
54  
55  
56  
57  
58  
59  
60
57. Shpaisman, N.; Sheihet, L.; Bushman, J.; Winters, J.; Kohn, J. One- Step Synthesis of Biodegradable Curcumin-Derived Hydrogels as Potent Soft Tissue Fillers After Brest Cancer Surgery. *Biomacromolecules* **2012**, *13*, 2279-2286.
58. James, K.; Levene, H.; Parsons, J. R.; Kohn, J. Small Changes in Polymer Chemistry have a Large Effect on the Bone-Implant Interface: Evaluation of a Series of Degradable Tyrosine-Derived Polycarbonates in Bone Defects. *Biomaterials* **1999**, *20*, 2203-2212.
59. Chang, L.; Deng, L.; Wang, W.; Lv, Z.; Hu, F.; Dong, A.; Zhang, Z. Poly(ethyleneglycol)-b-poly( $\epsilon$ -caprolactone-co- $\gamma$ -hydroxyl- $\epsilon$ - caprolactone) bearing pendant hydroxyl groups as nanocarriers for doxorubicin delivery. *Biomacromolecules* **2012**, *13*, 3301-3310.
60. Hu, X.; Liu, S.; Chen, X.; Mo, G.; Xie, Z.; Jing, X. Biodegradable Amphiphilic Block Copolymer Bearing Protected Hydroxyl Groups: Synthesis and Characterization. *Biomacromolecules* **2008**, *9*, 553-560.
61. Saulnier, B.; Ponsart, S.; Coudane, J.; Garreau, H.; Vert, M. Lactic Acid- Based Functionalized Polymers via Copolymerization and Chemical Modification. *Macromol. Biosci.* **2004**, *4*, 232-237.
62. Sudo, A.; Sugita, S. A Highly Rigid Diamine Monomer Derived from Naturally Occurring myo-Inositol and its Use for Polymer Synthesis. *J. Polym. Sci., Part A: Polym. Chem.* **2016**, *54*, 3436-3443.
63. Hahn, C.; Keul, H.; Moller, M. Hydroxyl-functional Polyurethanes and Polyesters: Synthesis, Properties and Potential Biomedical Application. *Polym Int.* **2012**, *61*, 1048-1060.
64. Begines, B.; Zamora, F.; Benito, E.; Garcia-Martin, M.; de. G.; Galbis, J. A. Conformationally Restricted Linear Polyurethanes from Acetalized Sugar-Based Monomers. *J. Polym. Sci., Part A: Polym. Chem.* **2012**, *50*, 4638-4646.
65. Japu, C.; Ilarduya, A. M. de.; Alla, A.; Jiang, Y.; Loos, K. Copolyesters Made from 1,4-Butanediol, Sebacic Acid, and D-Glucose by Melt and Enzymatic Polycondensation. *Biomacromolecules* **2015**, *16*, 868-879.
66. Lavilla, C.; Alla, A.; Ilarduya, A. M.de.; Guerra, S. M. High  $T_g$  Bio-Based Aliphatic Polyesters from Bicyclic D-Mannitol. *Biomacromolecules* **2013**, *14*, 781-793.
67. Wang, X.; Li, L.; Ye, X.; Wu, C. Comparative Study of Solution Properties of Amphiphilic 8-Shaped Cyclic-(Polystyrene-b-Poly(acrylic acid))<sub>2</sub> and Its Linear Precursor. *Macromolecules* **2014**, *47*, 2487-2495.
68. Cheng, F.; Su, T.; Luo, K.; Pu, Y.; He, B. The Polymerization Kinetics, Oxidation-responsiveness, and in Vitro Anticancer Efficacy of Poly(ester-thioether)s. *J. Mater. Chem. B.* **2019**, *7*, 1005-1016.
69. Zeng, X.; Zhang, Y.; Nystrom, A. Endocytic Uptake and Intracellular Trafficking of Bis-MPA-based Hyperbranched Copolymer Micelles In Breast Cancer Cells. *Biomacromolecules.* **2012**, *13*, 3814-3822.
70. Deshpande, U. N.; Jayakannan, M. Biotin Tagged Polysaccharide Vesicular Nanocarrier for Receptor Mediated Anticancer Drug Delivery in Cancer Cells. *Biomacromolecules* **2018**, *19*, 3572-3585.

1  
2  
3  
4  
5  
6 **For Table of Contents**  
7  
8  
9  
10  
11  
12  
13  
14  
15  
16  
17  
18  
19  
20  
21  
22  
23  
24  
25  
26  
27  
28  
29  
30  
31  
32  
33  
34  
35  
36  
37  
38  
39  
40  
41  
42  
43  
44  
45  
46  
47  
48  
49  
50  
51  
52  
53  
54  
55  
56  
57  
58  
59  
60

